Cdc42 is a key regulator of B cell differentiation and is required for antiviral humoral immunity

Marianne Burbage,[1] Selina J. Keppler,[1] Francesca Gasparrini,[1] Nuria Martínez-Martín,[1] Mauro Gaya,[1] Christoph Feest,[1] Marie-Charlotte Domart,[2] Cord Brakebusch,[3] Lucy Collinson,[2] Andreas Bruckbauer,[1] and Facundo D. Batista[1]

[1]Lymphocyte Interaction Laboratory, [2]Electron Microscopy Unit, London Research Institute, Cancer Research UK, London WC2A 3LY, England, UK
[3]Biomedical Institute, Biotech Research and Innovation Centre, University of Copenhagen, 2100 Copenhagen, Denmark

The small Rho GTPase Cdc42, known to interact with Wiskott–Aldrich syndrome (WAS) protein, is an important regulator of actin remodeling. Here, we show that genetic ablation of Cdc42 exclusively in the B cell lineage is sufficient to render mice unable to mount antibody responses. Indeed Cdc42-deficient mice are incapable of forming germinal centers or generating plasma B cells upon either viral infection or immunization. Such severe immune deficiency is caused by multiple and profound B cell abnormalities, including early blocks during B cell development; impaired antigen-driven BCR signaling and actin remodeling; defective antigen presentation and in vivo interaction with T cells; and a severe B cell–intrinsic block in plasma cell differentiation. Thus, our study presents a new perspective on Cdc42 as key regulator of B cell physiology.

CORRESPONDENCE
Facundo D. Batista:
facundo.batista@cancer.org.uk

Abbreviations used: AID, activation induced deaminase; BCR, B cell receptor; CD, cluster of differentiation; CTV, cell trace violet; dSTORM, direct stochastic optical reconstruction microscopy; GAP, GTPase activating protein; GEF, G nucleotide exchange factor; HEL, hen egg lysozyme; LatA, latrunculin A; NP, 4-hydroxy-3-nitrophenylacetyl hapten; SEM, scanning electron microscopy; S1P, sphingosine 1 phosphate; TEM, transmission electron microscopy; Tfh, T follicular helper cells; TIRF-M, total internal reflection microscopy; WAS, Wiskott-Aldrich Syndrome; WASp, WAS protein.

B cells provide a critical line of defense from pathogenic infections through the production of highly specific antibodies. The initial stages of B cell development occur in the bone marrow, where hematopoietic stem cells undergo stepwise rearrangements of the genes encoding the B cell receptor (BCR) and changes in the expression of cell surface receptors (Hardy et al., 1991). Immature B cells egress the bone marrow and migrate to the spleen to complete their development, going through transitional stages. Mature follicular B cells then recirculate throughout the body in search for cognate antigen, continually entering secondary lymphoid organs, including the LNs and spleen. Specific recognition of antigen by the BCR provides the first signal required for B cell activation. Typically, a second signal is required for maximal activation and is provided by $CD4^+$ helper T cells after the presentation of processed antigen on the B cell surface. These two signals in combination trigger the proliferation and differentiation of B cells, which go on to form antibody-secreting plasma cells and to establish germinal center responses for affinity maturation (Rajewsky, 1996).

B cell activation in vivo is predominantly triggered by antigen on the surface of a presenting cell (Batista and Harwood, 2009). The prevalence of this mode of activation has brought about a reevaluation of the importance of the cytoskeleton, given that the recognition of tethered antigen requires considerable alteration in B cell morphology (Fleire et al., 2006). Antigen-induced BCR signaling leads to radical reorganization of the actin cytoskeleton resulting in the modification of the BCR dynamics at the cell surface (Hao and August, 2005; Treanor et al., 2010; Treanor et al., 2011). Moreover the binding of membrane-bound antigen to cognate BCR triggers a cascade of intracellular signaling events that induces actin-dependent spreading of the B cell across the antigen-containing surface (Weber et al., 2008; Sohn et al., 2008; Depoil et al., 2008). However the mediators that link BCR signaling with reorganization of the actin cytoskeleton are currently not well defined.

The Rockefeller University Press $30.00
J. Exp. Med. 2015 Vol. 212 No. 1 53–72
www.jem.org/cgi/doi/10.1084/jem.20141143

Among actin regulators, the RhoGTPases are a highly conserved family that function as molecular switches by cycling between inactive GDP (guanosine diphosphate) and active GTP (guanosine triphosphate) bound states (Tybulewicz and Henderson, 2009). RhoGTPase activity is modulated by G-nucleotide exchange factors (GEF) that promote the formation of the GTP-bound state and binding to various effectors involved in actin reorganization. Conversely, GTPase-activating proteins (GAP) catalyze the hydrolysis of GTP and thereby switch off RhoGTPase activity. The importance of the RhoGTPases as a whole in the regulation of B cell responses is highlighted by the far-reaching consequences that impaired activity of several GEFs, such as Vav and DOCK8, has on humoral immune responses (Doody et al., 2001; Fujikawa et al., 2003; Randall et al., 2009; Zhang et al., 2009).

The importance of Rho GTPases in B cell physiology has been well established. For example, RhoA has been shown to regulate BCR signaling by influencing inositol-3 phosphate synthesis and calcium signaling (Saci and Carpenter, 2005). Moreover, B cell–specific inactivation of both Rac1 and Rac2 leads to virtually complete absence of B cells (Walmsley et al., 2003), and inactivation of Rac1 results in defects in spreading in transitional cells (Brezski and Monroe, 2007). However, although the inactivation of Rac2 leads to defects in B cell adhesion and synapse formation, it is unclear whether these proteins are involved in actin-dependent spreading in mature B cells (Arana et al., 2008).

Cdc42 has been little characterized in B cells, in spite of its proven chief role as an essential regulator of cell cycle (Johnson and Pringle, 1990), cell polarity (Etienne-Manneville, 2004), and actin cytoskeleton in other cellular systems. This is likely due, at least in part, to the reported mild phenotype of mice lacking Cdc42 in B cells (Guo et al., 2009) compared with the severe deficiencies observed in animals lacking Rac family members (Walmsley et al., 2003). However, the mild phenotype is somehow surprising given that Cdc42 directly or indirectly associates with Wiskott–Aldrich Syndrome Protein (WASp) and in complex with Arp2/3 regulates cytoskeleton remodeling (Symons et al., 1996; Aspenström et al., 1996; Kolluri et al., 1996). Importantly, mutations in WAS gene lead to a X-linked, recessive disease characterized by recurrent infections, abnormal lymphocyte function, as well as an increased risk for systemic autoimmunity (Derry et al., 1994; Sullivan et al., 1994). WASp deficient B cells play a primary role in driving autoimmunity (Becker-Herman et al., 2011). The Cdc42 effectors WASp and N-WASp have both been implicated the regulation of actin reorganization in response to BCR antigen engagement (Westerberg et al., 2012; Liu et al., 2013). Besides, expression of a dominant negative form of Cdc42 in B cells leads to alterations of the actin cytoskeleton (Westerberg et al., 2001). In addition, Cdc42 has been shown to play a role in the polarization and secretion of lysosomal protein involved in antigen extraction (Yuseff et al., 2011).

Here, we used a strategy harnessing the *mb1* promoter to generate mice with a selective and very effective deletion of Cdc42 in early B cell progenitors (Hobeika et al., 2006). Using this model, we demonstrated that Cdc42 plays an essential role in many aspects of B cell biology, including the formation of mature B cells and the establishment of antibody responses. We went on to dissect the underlying cause of the severe immunodeficiency of these mice and found that Cdc42-deficient B cells exhibit defects in BCR signaling and presentation of internalized antigen, leading to reduced B–T cell interactions and the absence of germinal center responses in vivo. Moreover, Cdc42-deficient B cells can normally proliferate and class switch when stimulated with CD40 or LPS, but they are completely impaired in their ability to differentiate into plasma cells. Together, these attributes render Cdc42-deficient mice unable to mount antibody responses after immunization with model antigen or viral infection, and highlight a fundamental role for this RhoGTPase in the regulation of B cell responses.

RESULTS

Cdc42 is required for efficient development of mature B cells

In the light of the emerging importance of the cytoskeleton in regulating B cell functions, we sought to characterize the role of the RhoGTPase Cdc42 during B cell development and activation in vivo. To do this, conditionally targeted $Cdc42^{flox/flox}$ mice were crossed with mice expressing Cre recombinase under the promoter of the *mb1* gene (Fig. 1 A; Wu et al., 2006; Hobeika et al., 2006). As *mb1* encodes the Igα subunit of the BCR, this approach circumvents limitations associated with gene targeting through the *Cd19* locus, which is known in some cases to lead to incomplete deletion, especially in the early B cell lineage (Rickert et al., 1997). Indeed, we observed that although Cdc42 was highly expressed early during B cell development in WT controls, expression was completely abrogated in $Cdc42^{flox/flox}$*mb1*$Cre^{+/-}$ mice (hereafter designated Cdc42 KO; Fig. 1 D).

To examine the impact of such an early deletion of Cdc42 on B cell development, bone marrow extracted from Cdc42 KO and WT mice was analyzed by multicolor flow cytometry and classified according to the Hardy classification system (Hardy et al., 1991). This method uses the differential expression of various cell surface markers as a read-out for the sequential stages during B cell development; for example, $B220^{+}CD43^{+}$ immature B cells are further divided into three populations (A–C) according to the expression of CD24 and BP-1. Overall bone marrow cellularity was not affected by Cdc42 deletion (unpublished data). In addition, we observed that the bone marrow of Cdc42 KO and WT mice have similar proportions of both immature cells ($B220^{+}CD43^{+}$), population A ($BP\text{-}1^{-}CD24^{-}$) and population B ($BP\text{-}1^{-}CD24^{+}$; Fig. 1, B and C). However, the Cdc42 KO mice exhibited a twofold lower proportion of population C ($BP\text{-}1^{+}CD24^{+}$) cells compared with WT control mice (Fig. 1 C). This indicates a partial block in the progression from stage B to C during B cell development, suggesting a role for Cdc42 in the early steps of preBCR expression. Despite this blockage, the number of B cell progenitors during subsequent stages of

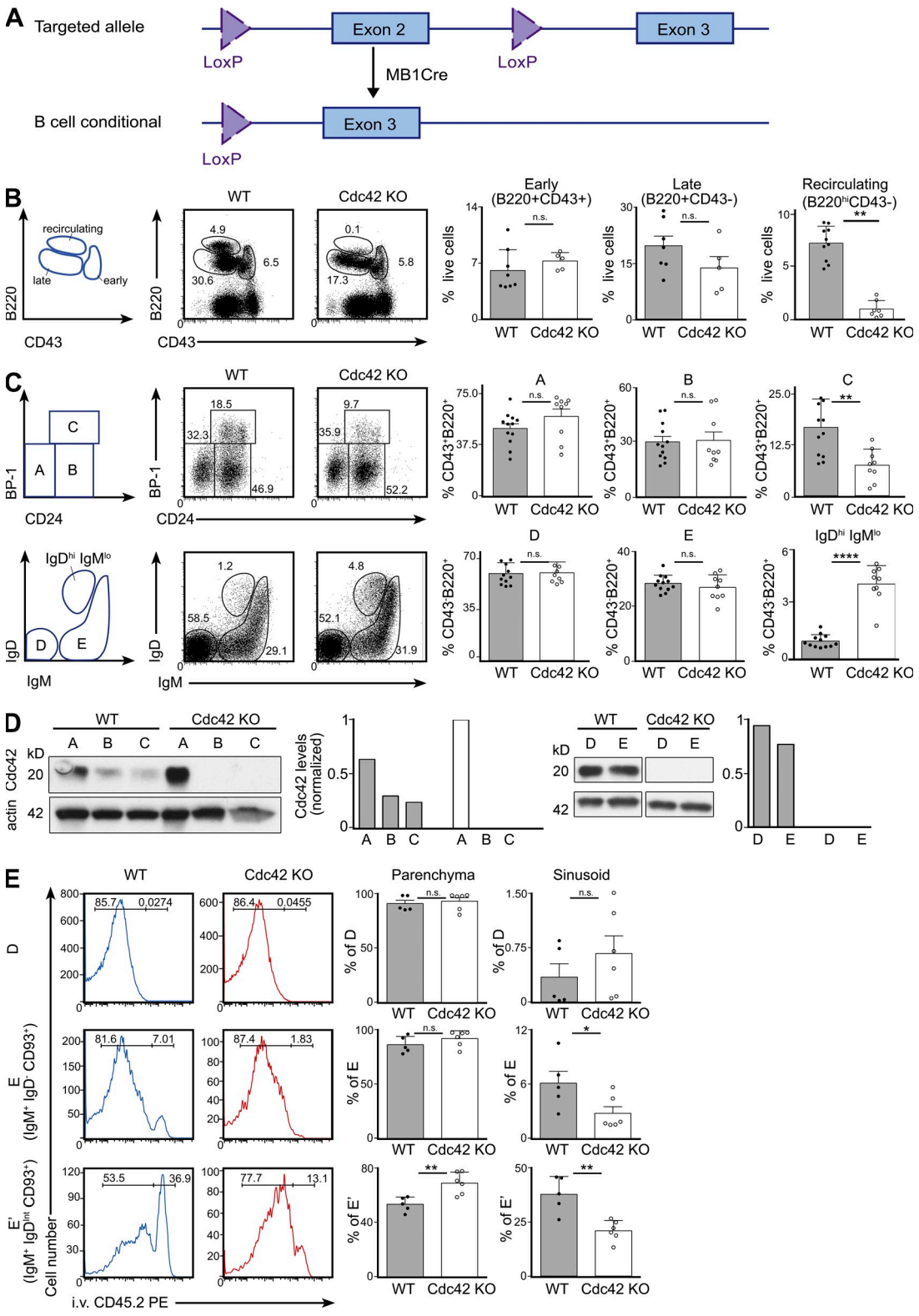

Figure 1. Cdc42 is important for early B cell development in the bone marrow. (A) Genetic approach used to ablate Cdc42 specifically in B cells. (B and C) Bone marrow from WT and Cdc42 KO mice was analyzed by flow cytometry. The gating strategies are shown on the left. B cell progenitors were divided into 3 populations on the basis of CD43 and B220 expression levels ($B220^+CD43^+$, $B220^+CD43^-$, and mature recirculating cells [$B220^{hi}CD43^-$]) as shown in B. They were further subdivided on the basis of CD24, BP-1, IgM, and IgD expression levels into populations A($B220^+CD43^+CD24^-BP\text{-}1^-$), B($B220^+CD43^+CD24^+BP\text{-}1^-$), C($B220^+CD43^+CD24^+BP\text{-}1^+$), D($B220^+CD43^-IgM^-IgD^-$), E($B220^+CD43^-IgM^+IgD^{-/lnt}$), and nonrecirculating.

development defined by IgM and IgD expression, (populations D and E) are comparable in Cdc42 KO and WT mice (Fig. 1 C). This recovery is presumably a result of successful proliferation after heavy chain rearrangements. Interestingly, the bone marrow of Cdc42 KO mice contains approximately four times more nonrecirculating $B220^{+}IgM^{lo}IgD^{hi}CD93^{+}$ B cells compared with WT animals (Fig. 1 C). In contrast, we found that Cdc42 KO mice exhibit around 10-fold fewer mature recirculating B cells (population F; $B220^{+}CD93^{-}CD43^{-}IgM^{+}IgD^{hi}$) compared with WT animals (Fig. 1 B). We wondered if this might be a result of impaired egress of these cells from the bone marrow in the absence of Cdc42.

To investigate the egress of immature B cells from the bone marrow, we used an in vivo pulse labeling procedure to reveal the distribution of developing B cells in Cdc42 KO mice (Pereira et al., 2009). This method involves selective labeling of populations according to their exposure to the blood, allowing the simultaneous identification and quantification of immature B cells in the bone marrow parenchyma and sinusoids. Using this approach, we observed that Cdc42 KO and WT mice exhibit a similar fraction of cells in populations A to D in the bone marrow parenchyma (Fig. 1 E, first row). In contrast, Cdc42 KO mice have higher levels of parenchymal immature IgD^{lo} B cells compared with WT mice, suggesting that the egress of immature IgD^{-} and IgD^{lo} cells from the bone marrow is specifically reduced in the absence of Cdc42 (Fig. 1 E). Moreover, we observed that the bone marrow sinusoids of Cdc42 KO mice contain threefold fewer IgD^{-} cells (Fig. 1 E, second row) and twofold fewer IgD^{lo} cells (Fig. 1 E, third row) than WT animals. As it is thought that hematopoietic cells exit the bone marrow through the sinusoids, this finding supports the notion of reduced egress of immature B cells in the absence of Cdc42.

In agreement with what was observed in the bone marrow, Cdc42 expression was abrogated in mature splenic B cells from Cdc42 KO mice as judged by Western blot (Fig. 2 A). In contrast, WT mature splenic B cells expressed high levels of Cdc42 (Fig. 2 A). We went on to quantify and visualize the various B cell populations in secondary lymphoid organs. The absence of Cdc42 resulted in a significant reduction in the number of mature B cells in the spleen and LNs, and in the absence of splenic marginal zone B cells ($B220^{+}CD21^{+}CD23^{-}$) in Cdc42 KO mice compared with WT animals (Fig. 2, B and C). Interestingly, we did not observe any accumulation of either T1 or T2 cells. Somewhat surprisingly, the deletion of Cdc42 also led to a significant accumulation of $CD21^{-}CD24^{-}$ B cells in the spleen (Fig. 2 B). Moreover, the development of the B1a and B1b populations in the peritoneal cavity was dramatically impaired in Cdc42 KO mice (unpublished data. Thus, it appears that Cdc42 plays an important role at several distinct stages in the development of mature B cell populations.

The localization of B cells within secondary lymphoid organs is important for their maturation. To examine whether the defects we observed in numbers of cells were caused by alterations in the organization of lymphoid organs, we imaged frozen sections of spleens and LNs taken from WT and Cdc42 KO mice using confocal microscopy. The relative distribution of B cells, T cells, and macrophages was visualized using antibodies against B220, TCR, and either F4/80 or CD169, respectively (Fig. 2, D and E). We observed that the organization of T cells and macrophages was not dramatically altered in the absence of Cdc42 in either spleen or LN (Fig. 2, D and E). As expected, the relative size and number of B cell follicles in both tissues was significantly lower in Cdc42 KO compared with WT mice (Fig. 2, D and E). However, it is important to note that the follicles that were formed after selective deletion of Cdc42 in B cells were found to contain follicular dendritic cells, suggesting the organization within these smaller follicles is not altered (unpublished data).

In conclusion, we have generated a mouse model with an efficient early deletion of Cdc42 in B cell progenitors. This model has allowed us to discern a thus far unappreciated role for Cdc42 in the earliest stages of B cell development, with the deletion of Cdc42 leading to a dramatic reduction in the total number of mature B cells and the absence of MZ and B1 cell populations.

Cdc42 in B cells plays a critical role in mounting antibody responses

Strikingly, during routine characterization of Cdc42 KO mice, we found that basal serum titers of IgM, IgG1, IgG2b, and IgG2c were almost undetectable (Fig. 3 A). This finding potentially indicates an underlying severe defect in antibody production and is in direct contrast with what has been reported in the $Cdc42^{flox/flox}CD19Cre^{+/-}$ model (Guo et al., 2009). In view of these diminished serum titers and the efficacy of deletion of Cdc42 in mature B cells in our Cdc42 KO mice, we went on to reexamine the role that this RhoGTPase plays in antibody responses to T cell–dependent antigen.

To do this, Cdc42 KO and WT mice were injected i.p. with the immunogenic hapten NP19-conjugated to KLH (NP19-KLH) in alum. NP-specific antibody titers in the serum were then quantified every week for 28 d using ELISA. During this time, we found that the primary IgM response in Cdc42

($IgD^{hi}B220^{+}CD43^{-}IgM^{+/int}IgD^{+}$) as shown in C. Quantifications are shown in the right-hand column and indicate percentage of cells in the indicated gates. Data were pooled from at least 4 independent experiments with at least 2 mice in each group. (D) B cell progenitors (A–E) were sorted from the bone marrow and protein expression of Cdc42 (first row) and actin (second row) were analyzed by Western blot. Densitometric analysis was used to quantify the signal intensity of Cdc42 normalized to actin and is shown in the chart below. (E) In vivo labeling of bone marrow progenitors. Intravenously injected anti CD45.2-PE was used to distinguish cells in BM sinusoid (PE^{+}) from cells in BM parenchyma (PE^{-}). The first two columns show a representative example of one WT mouse (blue) and one Cdc42 KO mouse (red). Populations D, E, and E' are shown. Quantification charts are shown in the two right-hand columns; data were pooled from three independent experiments with five mice in each group. *, $P < 0.05$; **, $P < 0.01$; ****, $P < 0.0001$.

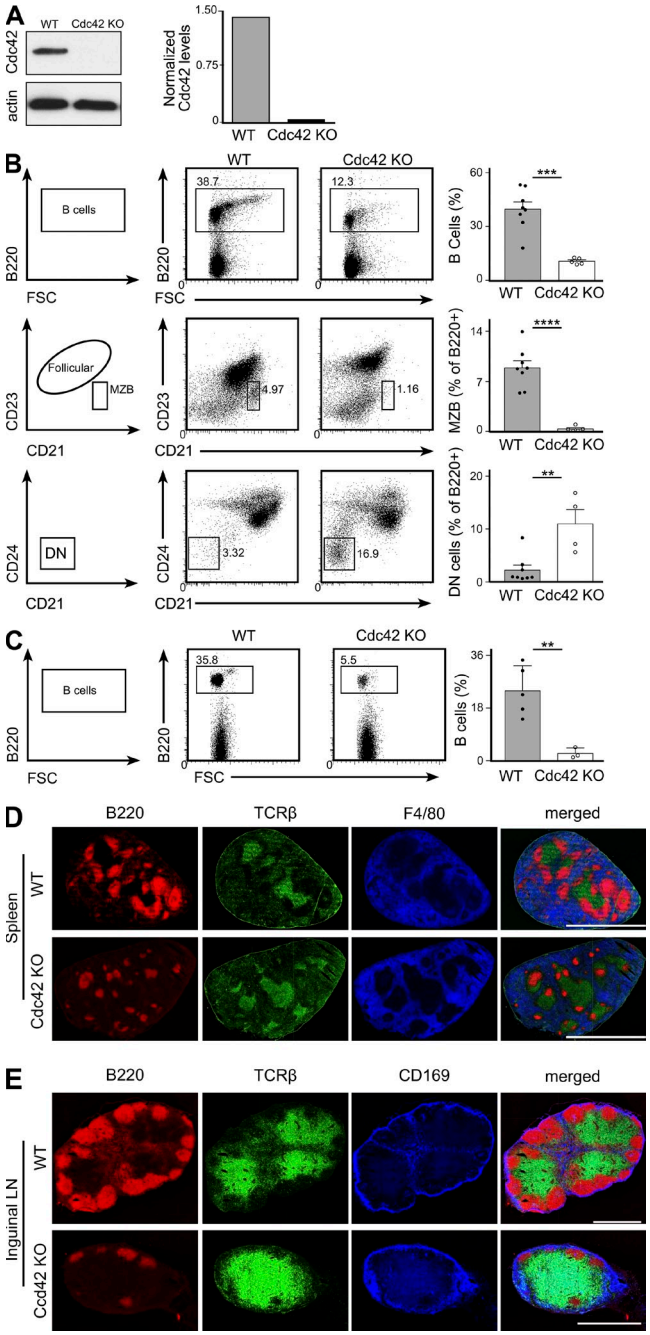

Figure 2. Cdc42 is essential to establish the mature B cell compartment. (A) Splenic WT and Cdc42 KO B cells were isolated and protein expression levels of Cdc42 (top row) and actin (bottom row) were analyzed by Western blot. Densitometric analysis was used to quantify the signal intensity of Cdc42 normalized to actin and is shown in the chart below. (B and C) Spleen (B) and inguinal LNs (C) from WT and Cdc42 KO mice were analyzed by flow cytometry. Gated populations are as follows: B cells (first row in B and C, $B220^+$), marginal zone B cells (second row, $B220^+CD21^{hi}CD23^{low}$), and double negative B cells (third row, $B220^+CD21^-CD24^-$). Quantification charts are shown in the right-hand column and represent percentage of live cells (first row in B and C) or percentage of $B220^+$ cells (second and third rows in B). (D–E) Frozen sections from spleens (D) or inguinal LNs (E) from WT and Cdc42 KO mice were stained with antibodies against B220, TCRβ, and F4/80 (D) or CD169 (E), and tiled images were acquired with a confocal microscope. Bars, 800 µm. Data were pooled from 3 experiments with $n = 8$ WT mice and $n = 4$ Cdc42 KO mice. Mean and SEM. *, $P < 0.05$; **, $P < 0.01$; ***, $P < 0.0001$; ****, $P < 0.0001$.

KO mice was at least 10-fold lower compared with WT mice (Fig. 3 B). Furthermore, in contrast to the mild differences described (Guo et al., 2009), the titers of all isotypes of NP-specific IgG antibodies were reduced by at least three orders of magnitude in animals lacking the expression of Cdc42 in B cells (Fig. 3 C). The dramatically reduced titers first establish a critical role for Cdc42 in the generation of antibodies after immunization; and second, imply the participation of this RhoGTPase in class switching during immune responses. This raises the question of whether the antibodies that were generated by Cdc42 KO after immunization had undergone affinity maturation. To determine this, we compared the extent to which the IgGs present in serum were able to bind to either NP3-BSA or NP23-BSA. Although higher affinity antibodies are capable of binding to either NP ligand, the lower affinity antibodies are only able to bind to NP23-BSA, providing a read-out for affinity maturation. We found that NP-specific antibodies in post-immunization serum of WT mice were able to bind both NP3-BSA and NP23-BSA. In contrast, the antibodies present in the serum of Cdc42 KO mice were only able to bind to the NP23-BSA ligand, demonstrating that they had not undergone affinity maturation after immunization (Fig. 3 D).

Unlike previous studies, it is clear from these experiments that Cdc42 plays a fundamental role in B cell function; specifically, in terms of antibody generation and affinity maturation in response to T cell–dependent antigens. Importantly, the lower number of mature B cells formed in Cdc42 KO mice alone may not be a sufficient explanation for this given the severity in the reductions of the antibody responses observed.

Cdc42 is required for antibody responses and germinal center formation during infection

In view of the importance of Cdc42 in response to NP-KLH, we went on to investigate the impact of Cdc42 deletion on response to viral infection. Cdc42 KO and WT mice were infected with Influenza A and the levels of antibodies in the serum were quantified using ELISA. 9 d after infection, we detected high titers of specific IgM and IgG antibodies in the serum of WT mice, but dramatically reduced titers of influenza-specific IgM and undetectable levels of IgG in the serum of Cdc42 KO mice (Fig. 4 A). These differences clearly demonstrate the principal importance of Cdc42 during B cell activation in response to infection.

To obtain a more detailed understanding of this impaired antibody response, we used a combination of flow cytometry and confocal microscopy to examine the LNs and spleens of WT and Cdc42 KO mice after infection. In response to influenza A, both WT and Cdc42-deficient mice display

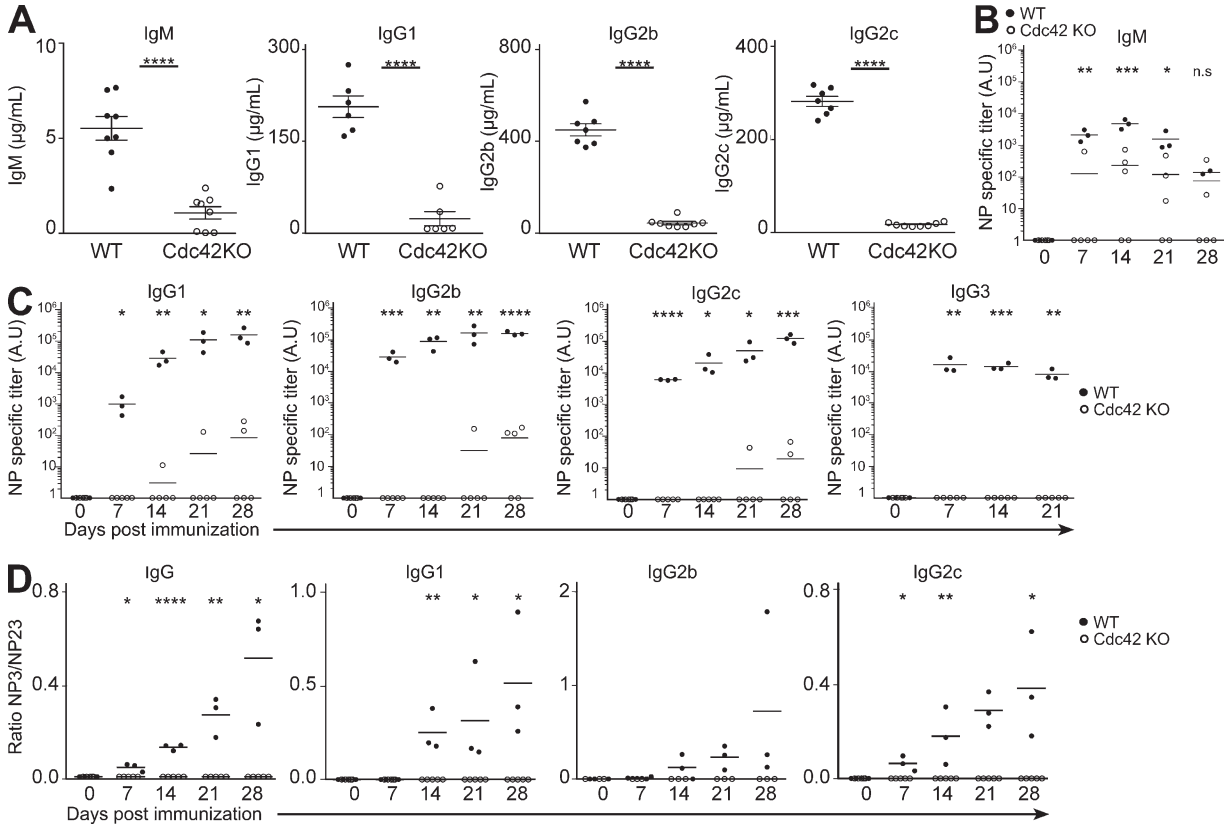

Figure 3. Cdc42 is essential for antibody responses to NP-KLH. (A) Serum from WT and Cdc42 KO mice was collected and Ig (IgM, IgG1, IgG2b, and IgG2c) levels were measured by ELISA. Data are representative of more than two independent experiments with at least three mice in each group. (B and C) WT and CDc42 KO mice were immunized with NP-KLH in alum. NP_{23}-specific IgM (B) or IgG1, IgG2b, IgG2c, and IgG3 (C) titers were measured by ELISA. Graphs represent NP-specific titers in WT (black dots) or Cdc42-KO (clear dots). (D) ELISA analysis showing affinity maturation of total IgG and IgG1, IgG2b, or IgG2c isoforms in response to NP-KLH in WT and Cdc42 KO mice, expressed as the ratio of NP3 to NP23. Data are representative of 2 independent experiments with at least 3 animals in each group. Mean and SEM. Student's *t* test. *, P < 0.05; **, P < 0.01; ***, P < 0.0001; ****, P < 0.00001.

a comparable increase in the number of $IgD^{lo}CD138^{int}$ plasmablasts (Fig. 4 B). However, the formation of $CD138^{hi}$ plasma cells observed in WT animals was abrogated in Cdc42 KO mice after infection (Fig. 4 B), reflecting the trend in the serum antibody titers (Fig. 4 A). Indeed, the strong intracellular anti-kappa staining detected in frozen spleen sections from WT mice was absent in Cdc42 KO mice (Fig. 4 C), suggesting that Cdc42 is required for the formation of IgM-secreting extrafollicular plasma cells that arise rapidly after infection. Importantly, WT mice form germinal centers after infection, as indicated by a $CD95^+GL7^+$ population using flow cytometry and $Bcl6^+$ population in spleen sections (Fig. 4, D and E). In contrast, Cdc42 KO mice do not form germinal centers in response to infection with influenza (Fig. 4, D and E) explaining the dramatic reduction in IgG titers observed in these animals. As such, it appears that Cdc42 plays a critical role in mounting antibody-specific responses to infection and is involved in both the formation of extracellular plasma cells and establishment of germinal centers.

The formation of germinal center cells is associated with the appearance of follicular T helper cells (Tfh; Vinuesa and Cyster, 2011). After Influenza infection in WT mice, we were able to observe a define Tfh population ($CD4^+$ $CXCR5^+$ $PD1^+$), which was drastically reduced in Cdc42 KO mice (Fig. 4 F). To establish that the lack of germinal center observed in the Cdc42 KO is an intrinsic B cell defect and not the result of an abnormal Tfh response, we took advantage of bone marrow chimeras. To this end, WT CD45.1 hosts were reconstituted with WT CD45.1 and Cdc42 KO CD45.2 cells. 12 wk after reconstitution, these mice were infected with 200 PFU Influenza and analyzed as above. As expected, a robust Tfh (Fig. 4 G) response was measured in these animals. Noticeably, we observed that only WT B cells were able to form germinal centers. Altogether, these results demonstrate that the inability of Cdc42 KO B cells to form humoral immune responses is an intrinsic B cell defect.

Cdc42 participates in mediating early signaling during B cell activation

The important role that we have identified for Cdc42 in antibody generation raises the question of the underlying molecular mechanism by which this RhoGTPase mediates these effects. To dissect this, we initially examined the function of Cdc42 during the early signaling events that occur upon BCR stimulation.

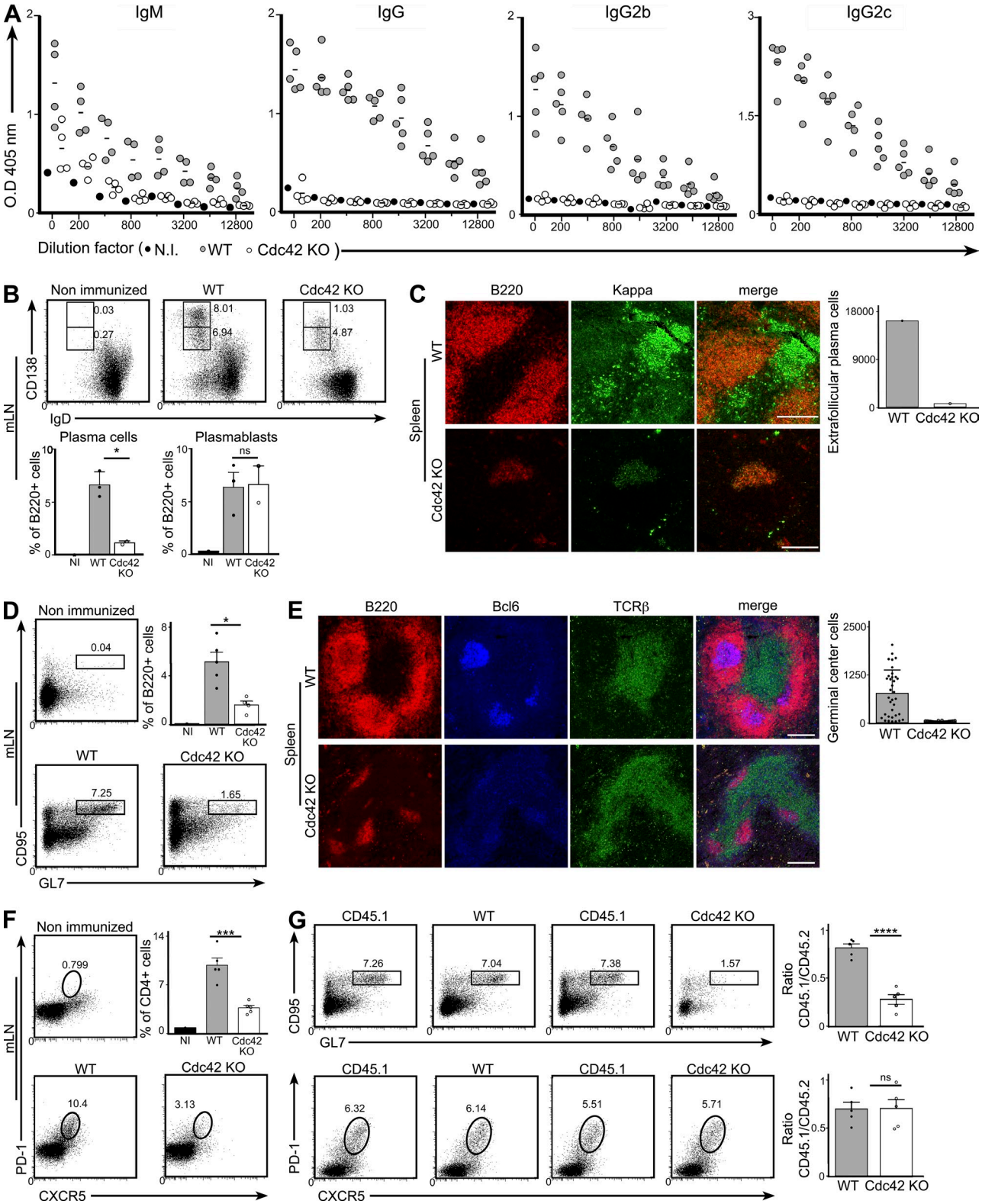

Figure 4. Cdc42 is essential to achieve responses against viral infection WT and Cdc42 KO mice were infected with Influenza A virus and immune responses were analyzed at day 9 after infection. (A) Influenza-specific antibody titers were measured by ELISA. Serial dilutions of the sera are shown. (B, D, and F) Mediastinal LNs from WT and Cdc42-KO mice were analyzed by flow cytometry 9 d after infection. Plasmablasts (B; IgD^{lo} $CD138^{Int}$), plasma cells (B; IgD^{lo} $CD138^{hi}$), germinal center cells (D, $B220^{+}CD95^{+}GL7^{+}$) or Tfh cells (F, $PD\text{-}1^{+}CXCR5^{+}$) are shown. (C–E) Tile images of spleen sections were acquired and show extrafollicular plasma cells (C; intracellular anti-κ staining) or germinal center cells (E; $Bcl6^{+}$ cells). Quantification charts

The ability of B cells to sense antigen is tightly associated with their morphology and the organization of the actin cytoskeleton. By scanning electron microscopy we observed that Cdc42 KO B cells had less membrane ruffles than WT cells (Fig. 5 A). Consistent with this observation, Cdc42 KO had a lower content in filamentous actin (Fig. 5 B). Recent studies have highlighted the relationship between actin cytoskeleton, BCR dynamics and also BCR nanoscale organization on the ability of B cells to signal. We therefore analyzed the nanoscale organization of the IgM-BCR with the super-resolution microscopy technique dSTORM. We noticed that the average radius of IgM nanoclusters, as suggested by the H function (Kiskowski et al., 2009), was increased in Cdc42 KO cells as compared with WT cells (Fig. 5 A).

To investigate the role of Cdc42 in the context of B cell activation, we used a GTP pull-down assay to visualize the activation status of Cdc42 after antigenic stimulation. As shown in Fig. 5 C, Cdc42 was activated within one minute after BCR cross-linking and returned to prestimulation levels within 15 min. This activation kinetic implicates Cdc42 in the early events after BCR activation, so we went on to investigate the impact that deletion of Cdc42 has on the activation of other canonical mediators involved in BCR signaling. To this end, the phosphorylation status of different signaling molecules was examined using flow cytometry. As shown in Fig. 5 (D and F), 2 min after BCR cross-linking, WT B cells exhibit increased levels of phosphorylation of Src, Syk, ERK, and Akt compared with prestimulation. In contrast, the increase in phosphorylation of these mediators was significantly lower in Cdc42 KO B cells (Fig. 5, D and F, and Fig. S2 B). Phosphorylation of the co-receptor CD19 was also reduced in Cdc42 KO B cells (Fig. 5 G). In line with this, Cdc42 KO B cells were less able to initiate calcium signaling compared with WT cells in response to both BCR cross-linking and cytoskeleton disruption with LatA (Fig. 5 E).

In a physiological context, the early signaling events after BCR stimulation by membrane-bound antigen trigger the reorganization of the actin cytoskeleton such that the B cell spreads across the presenting cell surface. This cellular response allows the B cell to maximize the amount of antigen gathered and its aggregation into a central cluster before internalization. To investigate how Cdc42 might be involved in the cytoskeleton reorganizations required for B cell spreading, we used planar lipid bilayers loaded with antibody against the BCR as surrogate antigen. WT and Cdc42 KO B cells were settled on bilayers and the extent of antigen microcluster formation and spreading were visualized by live TIRF microscopy. As expected, WT B cells spread over the antigen containing surface, forming antigen microclusters within the first three minutes, followed by a slower contraction phase during which antigen is gathered in a central cluster (Fig. 5 H and Video 1). Although Cdc42 KO B cells were able to form some antigen microclusters, the ability of these cells to spread was dramatically compromised (Fig. 5 H and Video 2). In line with this, Cdc42 KO B cells were also less able to spread on coverslips with immobilized antigen as indicated by the considerably altered morphology visible in both TIRF (phalloidin staining) and SEM images (Fig. 5 I). These defects support the notion that Cdc42 regulates actin reorganization after BCR stimulation.

In view of the impaired early BCR signaling and aberrant actin reorganizations in Cdc42-deficient B cells, we speculated that these cells might be less able to internalize antigen through the BCR. To test this hypothesis, ice-cold B cells were loaded with saturating amounts of biotinylated anti-IgM and then washed to remove unbound antibody. Then, the remaining amount of anti-IgM on the B cell surface was quantified using fluorescently labeled streptavidin at defined points during the subsequent 30 min. Somewhat surprisingly, the rate and extent to which WT and Cdc42 KO B cells internalize IgM-BCR was not significantly different (Fig. 5 J). Titration of the amount of anti-IgM used to stimulate the B cells did not reveal any significant difference between WT and Cdc42 KO cells (unpublished data). Similar experiments performed with anti-IgM–coated microspheres indicated that Cdc42 KO B cells are also able to internalize particulate antigen, albeit with a slight delay (unpublished data). The results from these internalization assays strongly suggest that the defects in early BCR signaling and actin reorganization are not sufficient to explain the dramatically reduced antibody generation observed in Cdc42 KO mice after immunization.

Cdc42 is required for B cells to present antigen to T cells

Effective B cell activation requires signaling through the BCR, as well as the receipt of a second signal from helper $CD4^+$ T cells. After BCR-mediated internalization, antigen is targeted to a specific polarized cellular compartment where it is loaded onto MHCII for presentation to T cells. This compartment is rapidly polarized after antigen internalization (Siemasko et al., 1998). As Cdc42 is known to regulate polarity in a variety of cells, it seems likely that it might be involved in mediating the polarization of internalized antigen in B cells and, as a result, impact the subsequent efficacy of antigen presentation to T cells.

To investigate a possible role for Cdc42 in determining the polarization of internalized antigen, Cdc42 KO and WT B cells were stimulated with fluorescently labeled anti-IgM for 30 min before fixation and imaging using confocal microscopy. In line with previous observations, ~75% of stimulated WT B cells display polarization of the antigen-containing

of spleen sections are shown in the right-hand columns of C and E. Bar, 200 µm. Data are representative of three independent experiments with at least 3 mice in each group. (G) Mixed bone marrow chimeras (either 50:50 WT CD45.1:WT CD45.2 or 50:50 WTCD45.1:Cdc42 KO CD45.2) were infected with Influenza virus, and mLNs were analyzed by flow cytometry. Germinal center ($B220^+CD95^+GL7^+$) and Tfh ($PD\text{-}1^+CXCR5^+$) cells are shown. Quantification charts are shown in the right-hand column and indicate the ratio between CD45.1 and CD45.2 cells in each population.

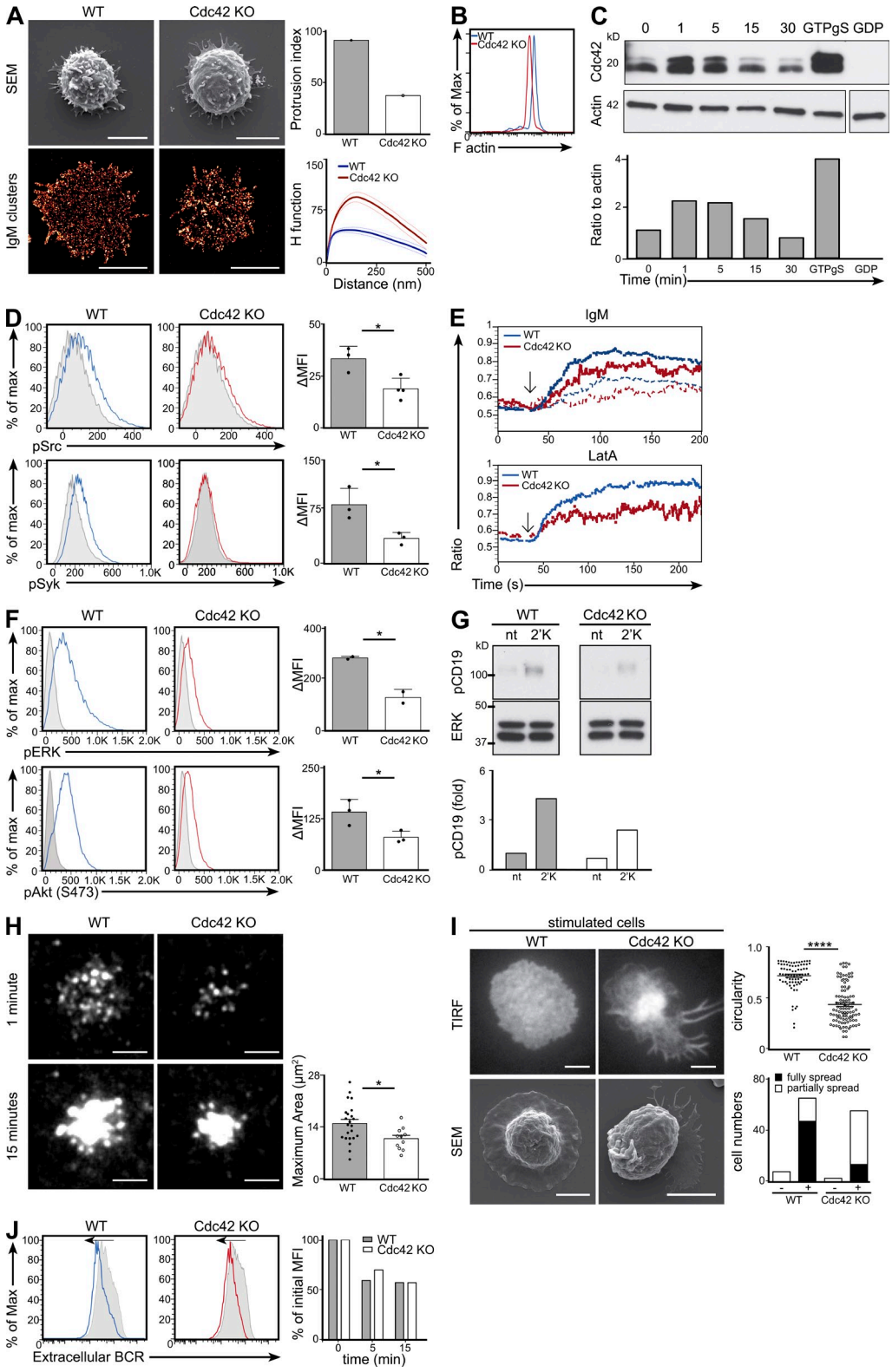

Figure 5. Cdc42 plays a role in early BCR signaling. (A) Purified splenic Cdc42 KO and WT B cells were settled on TIB120-coated coverslips. Representative scanning electron microscopy images (top row) and direct stochastic optical reconstruction microscopy for IgM nanoscale organization are shown (bottom row). Quantifications were performed on at least 50 cells and are shown in the right-hand columns and show the percentage of cells with more than 30 protrusions and the H function (see text). Data are representative of two independent experiments. (B) Purified splenic WT and Cdc42 KO B cells were stained intracellularly with phalloidin and analyzed by flow cytometry. Data are representative of 3 independent experiments. (C) Purified

compartment (Fig. 6 A). In contrast, B cells obtained from Cdc42 KO mice were significantly less able to polarize internalized antigen (Fig. 6 A). This suggests that Cdc42 is involved in the organization of the antigen-containing compartment.

We moved on to examine if the altered intracellular organization of antigen in Cdc42 KO B cells has a corresponding impact on the capacity of these cells to present that antigen to helper T cells. To explore this in vitro, we took advantage of the Eα peptide presentation assay to assess the amount of specific peptide-MHC present on the B cell surface after BCR stimulation. Cdc42 KO and WT B cells were incubated for 5 h with microspheres coated with anti-IgM and increasing concentrations of the peptide Eα (Rudensky Ayu et al., 1991). The amount of Eα-MHC on the B cell surface was then visualized by flow cytometry using an antibody recognizing the Eα peptide bound to MHCII ($I\text{-}A^b$). The total surface expression of MHCII increased to a similar extent in WT and Cdc42 KO cells (unpublished data). Strikingly, antigen presentation on the surface of Cdc42-deficient B cells was dramatically impaired compared with WT, even using particles coated with the highest concentration of Eα peptide (Fig. 6 B). To assess the impact of this reduction on T cell activation, we used $CD4^+$ T cells purified from OTII mice that express a TCR specific for a peptide of OVA. CFSE-labeled Cdc42 KO and WT B cells were stimulated with microspheres coated with anti-IgM and various concentrations of OVA before incubation with CTV-labeled OTII T cells. After 3 d, flow cytometry was used to quantify the proliferation of both B and T cells by respective dilution of the cytoplasmic dyes CFSE and CTV. Co-culturing stimulated WT B cells with OTII T cells triggered intense proliferation in both populations as a result of successful antigen presentation (Fig. 6 C). In contrast, the capacity to trigger both B and OTII T cell proliferation was substantially diminished using B cells purified from Cdc42 KO mice (Fig. 6 C). These results demonstrate that the impaired polarization of internalized antigen in Cdc42 KO B cells correlates with a diminished antigen presentation to T cells in vitro. As a consequence, B cells are less able to obtain efficient T cell help, making them less likely to receive the necessary activatory signals to undergo proliferation in the absence of Cdc42.

To examine the impact of Cdc42 deletion on the behavior of B cells in vivo, Cdc42 KO and WT B cells were adoptively transferred into WT recipient mice. After 24 h, both Cdc42 KO and WT B cells were found in explanted inguinal and popliteal LNs using two-photon microscopy. Although WT B cells moved at mean speeds of 5 μm/min, in agreement with previous studies (Miller et al., 2002), Cdc42 KO B cells were significantly slower, with a mean speed of 3 μm/min (Fig. 6 E and Video 3). Given that Cdc42 KO move over a shorter distance during the acquisition period, this indicates that Cdc42 may be involved in mediating cell migration in vivo.

To evaluate the role of Cdc42 during B cell activation in vivo, we crossed Cdc42 KO mice with MD4-Tg mice whose B cells express a BCR with high affinity for hen egg lysozyme (HEL; Goodnow et al., 1988) to generate HEL-specific B cells lacking Cdc42 (HEL-Cdc42 KO). HEL-Cdc42 KO or HEL-WT B cells were adoptively transferred along with OTII T cells into WT recipients before footpad administration of microspheres coated with HEL and OVA. 24 h later, whole popliteal LNs of recipient mice were explanted, fixed, and examined using two-photon microscopy. WT and Cdc42 KO B cells were found in similar regions of the LN (Fig. 6 D), indicating that both are able to undergo CCR7-dependent migration toward the B–T cell border after antigen stimulation (Okada et al., 2005). We then went on to visualize the formation of B–T cell conjugates in freshly isolated popliteal LNs after administration of HEL-OVA coated microspheres.

splenic WT B cells were stimulated with 10 $\mu g.ml^{-1}$ anti-IgM $F(ab')_2$ for different times and lysed. Nonstimulated lysates incubated with GTPgS (positive) or GDP (negative) were used as controls. Lysates were incubated with GST-PAK beads (binding to Cdc42-GTP) and both total lysate and the bound fraction were analyzed by Western blot. Cdc42-GTP (top row) and actin (bottom row) protein levels are shown. Densitometric analysis was used to quantify the signal intensity of Cdc42-GTP normalized to actin. Data are representative of at least 3 independent experiments. (D and F) Flow cytometry analysis for levels of pSrc and pSyk (D), or pErk and pAkt (F) in purified splenic WT (blue lines) or Cdc42 KO (red lines) B cells at steady state (gray shaded histogram) or 2 min after stimulation with 10 $\mu g\ ml^{-1}$ anti-κ light chain (colored lines). Quantifications are shown in the right column and were calculated as the difference between the geometric mean of the fluorescence between stimulated and nonstimulated samples (ΔMFI). Data are representative of >3 independent experiments. (E) Intracellular Ca^{2+} influx in purified splenic WT (blue lines) or Cdc42 KO (red lines) B cells after stimulation with either anti-IgM $F(ab')_2$ (top; 1 $\mu g\ ml^{-1}$ [dotted lines], 10 $\mu g\ ml^{-1}$ [solid lines]) or latrunculin A (bottom; 1 $\mu mol/liter^{-1}$). Data are representative of two independent experiments. (G) Western blot analysis showing protein levels of phospho-CD19 (top) and ERK (bottom) in splenic WT or Cdc42 KO B cells after stimulation with 10 $\mu g.ml^{-1}$ anti-κ light chain antibody. Densitometric analysis was used to quantify the signal intensity of pCD19 normalized to ERK, referred to the respective controls. Quantification is shown in the chart below. (H) Representative images by total internal reflection microscopy (TIRF) of splenic WT (left column) or Cdc42 KO B cells (right column) settled on planar lipid bilayers loaded with Alexa Fluor 633-streptavidin and anti-κ light chain antibody. Representative images were taken at 1 and 15 min after settling and show the spreading (top row) and contraction (bottom row) phases. Quantification chart in the right-hand column indicates maximum spreading area. Data are representative of 3 independent experiments. (I) Representative TIRF (top row) and SEM (bottom row) of WT (left column) and Cdc42 KO (right column) splenic B cells stimulated on glass coverslips coated with anti-κ light chain antibody for 10 min, before fixation and staining with phalloidin for TIRF or processing for SEM. Quantifications (right column) were performed on >100 cells and indicate circularity index calculated with Image J (top right) and percentage of fully spread cells (bottom right). Data are representative of 3 independent experiments. (J) Internalization of soluble anti-IgM antibody measured by flow cytometry in WT (blue line) or Cdc42 KO splenic B cells (red line) after 15 min of stimulation with biotinylated anti-IgM antibody. Gray shaded histograms indicate basal IgM levels. The right-hand chart shows internalization kinetics. Data are representative of >3 independent experiments. (Bars, 3 μm). Error bars are mean ± SEM. Student's *t* test. *, $P < 0.05$; **, $P < 0.01$; ***, $P < 0.0001$; ****, $P < 0.00001$. All charts are representative of at least 3 independent experiments.

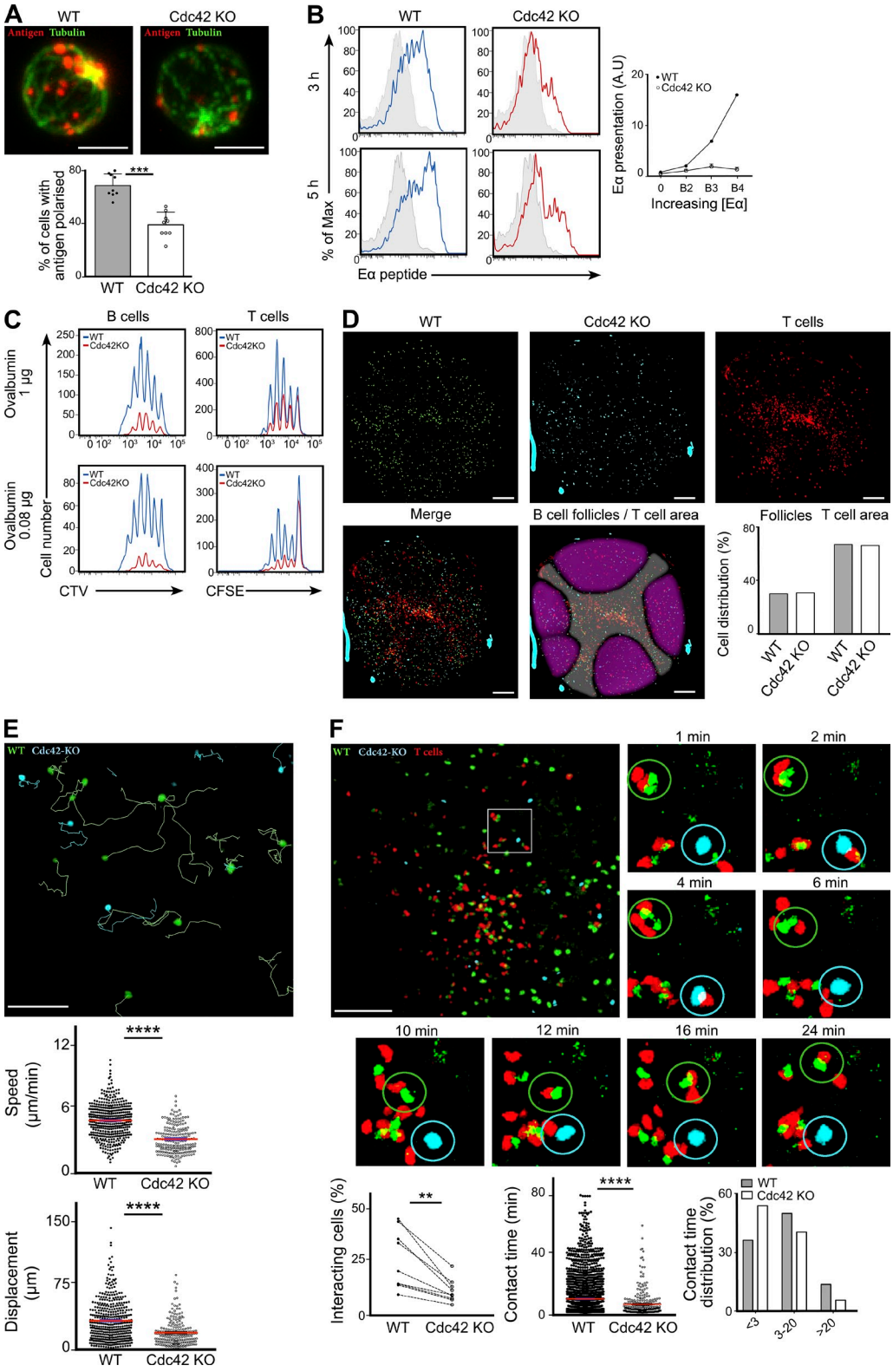

Figure 6. Cdc42 is essential for antigen presentation. (A) Representative confocal microscopy (with a 63× objective) images showing internalized Alexa Fluor 647 anti-IgM antibody in WT (left) or Cdc42 KO (right) splenic B cells. Bars, 3 µm. Quantification (bottom) indicates percentage of cells with polarized antigen per field of view, each image containing at least 10 cells. Data are representative of 3 independent experiments. (B) Antigen presentation assay showing presentation of Eα peptide on MHCII measured by flow cytometry. Splenic WT (left, blue line) and Cdc42 KO (right, red line) B cells were loaded with beads coated with anti-IgM antibody and Eα peptide and cultured for 3 h (top) or 5 h (bottom). Quantification (right) indicates ratio

In line with in vitro observations, we observed that HEL-Cdc42 KO B cells formed significantly fewer conjugates with OTII T cells compared with WT B cells (Fig. 6 F and Video 4). Moreover, it was clear that HEL-Cdc42 KO B cells exhibit a shorter overall contact time with OTII T cells compared with WT B cells (Fig. 6 F and Video 4). This demonstrates that Cdc42-deficient B cells are less able to present antigen to cognate T cells, suggesting this RhoGTPase is involved in mediating the efficient presentation of internalized antigen for B cell activation in vivo.

Together, these in vitro and in vivo results establish a role for Cdc42 in the polarization and subsequent presentation of internalized antigen by B cells.

Cdc42 in B cells is essential for the formation of plasma cells

Thus far we have identified roles for Cdc42 in mediating the two signals required for B cell activation. Although these defects likely contribute to the immune-deficient phenotype of the Cdc42 KO mouse, the severity of the observed reduction in antibody serum titers made us question whether there might be an underlying intrinsic problem for B cells in the formation of plasma cells in the absence of Cdc42 expression.

To investigate this issue, Cdc42 KO and WT B cells were provided with either CD40L or LPS (in the presence of IL-4 and I-L5) to override the observed defects in B cell activation in vitro. After 4 d, we observed that both Cdc42 KO and WT B cells underwent comparable, extensive proliferation and class switch recombination (CSR), predominantly to IgG1 (Fig. 7, A and B). In addition, we found that WT B cells form $CD138^{hi}$ plasma cells and can secrete large amounts of immunoglobulins into the culture supernatant. In contrast, Cdc42 KO B cells formed 10-fold fewer $CD138^{hi}$ plasma cells and the levels of immunoglobulin produced were below the threshold for detection (Fig. 7, C and D). As such, it appears that although Cdc42 in B cells is not essential for CSR, the process of plasma cell formation is dramatically impaired in its absence. To further investigate this role for Cdc42, WT and Cdc42 KO B cells were stimulated with LPS (in the presence of IL4 and IL5). After 4 d, the resulting cells were sorted using flow cytometry on the basis of CD138 and IgG1 expression. Three different populations, namely $IgG1^{hi}$, $CD138^{hi}$, and $IgG1^{-}CD138^{lo}$ cells, were then processed for transmission electron microscopy (TEM) to investigate ultrastructural features. As expected, WT $CD138^{hi}$ plasma cells exhibit an expanded endoplasmic reticulum (ER) typical of cells specialized for large-scale antibody production and WT $IgG1^{+}$ cells display more classic B cell morphology with a relatively large nucleus and small cytoplasm (Fig. 7 E). We observed that though there were no visible differences in the $IgG1^{+}$ population, Cdc42 KO B cells did not form a detectable $CD138^{hi}$ plasma cell population. Moreover, although more than half of the WT $IgG1^{-}CD138^{lo}$ B cell population contained an expanded ER, this was present in only 5% of the Cdc42 KO $IgG1^{-}CD138^{lo}$ B cells. Thus, the ultrastructure of activated B cells further supports the notion that Cdc42 is required for the differentiation of plasma cells.

To understand the molecular signaling pathways underlying such a dramatic block in plasma cell differentiation, we evaluated the activation status of a range of intracellular mediators in response to CD40L in WT and Cdc42 KO B cells. Several signaling pathways and mediators, such as the PI3K pathway, and Erk and STAT3, have been shown to be important during plasma cell differentiation (Omori et al., 2006; Yasuda et al., 2011). In WT B cells, CD40L stimulation triggers the activation of the PI3K signaling pathway, resulting in the rapid phosphorylation of Akt and FoxO1 (Fig. 8 A). Furthermore, this stimulation also causes phosphorylation and activation of ERK, STAT3, and the PAK kinase (Fig. 8 A), demonstrating that WT B cells mediate the intracellular signaling required for plasma cell formation. In contrast, we observed that Cdc42 KO B cells are unable to trigger the PI3K signaling pathway and are severely impaired in phosphorylation of ERK, STAT3, and PAK kinase in response to CD40L stimulation (Fig. 8 A). These results highlight the importance of Cdc42 in mediating the intracellular signaling that is required for the formation of plasma cells.

Finally, we examined whether the RhoGTPase Cdc42 is involved in shaping the expression levels of the *prdm1* gene encoding the transcriptional repressor Blimp1. The

between mean Eα fluorescence and total MHCII fluorescence. Data are representative of 2 independent experiments. (C) Proliferation profiles of B (left column) and T cells (right column) by flow cytometry. OTII T cells were co-cultured for 3 d with purified WT (blue line) or Cdc42 KO (red line) B cells loaded with anti-IgM- and ovalbumin-coated beads (at the concentrations noted). Data are representative of 2 independent experiments. (D) Representative two-photon microscopy image of a whole fixed popliteal LN after adoptive transfer of HEL-WT B cells (green), HEL-Cdc42 KO B cells (cyan), and OTII T cells (red) into WT mice, and subsequent immunization with Hel- and OVA-coated beads. B cell follicles and T cell area were highlighted in magenta and gray for illustrative purposes. The proportion of cells in B cell follicles versus T cell area were measured and quantification is shown in the chart (bottom right). Bars, 150 µm. Data are representative of 2 independent experiments. (E) Representative image of the visualization of homeostatic movement of WT (green) and Cdc42 KO (cyan) cells by two-photon microscopy. Representative tracks are shown on the image. Quantifications are shown below and indicate the mean speed over the span of the video as well as the mean displacement of cells. Data are representative of 2 independent experiments. (F) Representative images of the whole field of view (left) as well as higher magnification images (7×) of the visualization of B–T cell interactions in explanted LNs by two-photon microscopy. SNARF-1–labeled OTII T cells (red), CFSE-labeled HEL-WT (green), and CTV-labeled $MD4^{+}$ Cdc42 KO (cyan) B cells were adoptively transferred into WT recipients, which were then immunized intra-footpad with Hel- and OVA-coated beads. Popliteal LNs were explanted and imaged 15 h after immunization. Quantifications are shown below and represent the percentage of B cells interacting with T cells over the span of the video, as well as the mean length and the distribution of the contact time of B–T cell interactions. Data are representative of 3 independent experiments. Mean and SEM. Student's *t* test. *, $P < 0.05$; **, $P < 0.01$; ***, $P < 0.0001$; ****, $P < 0.00001$.

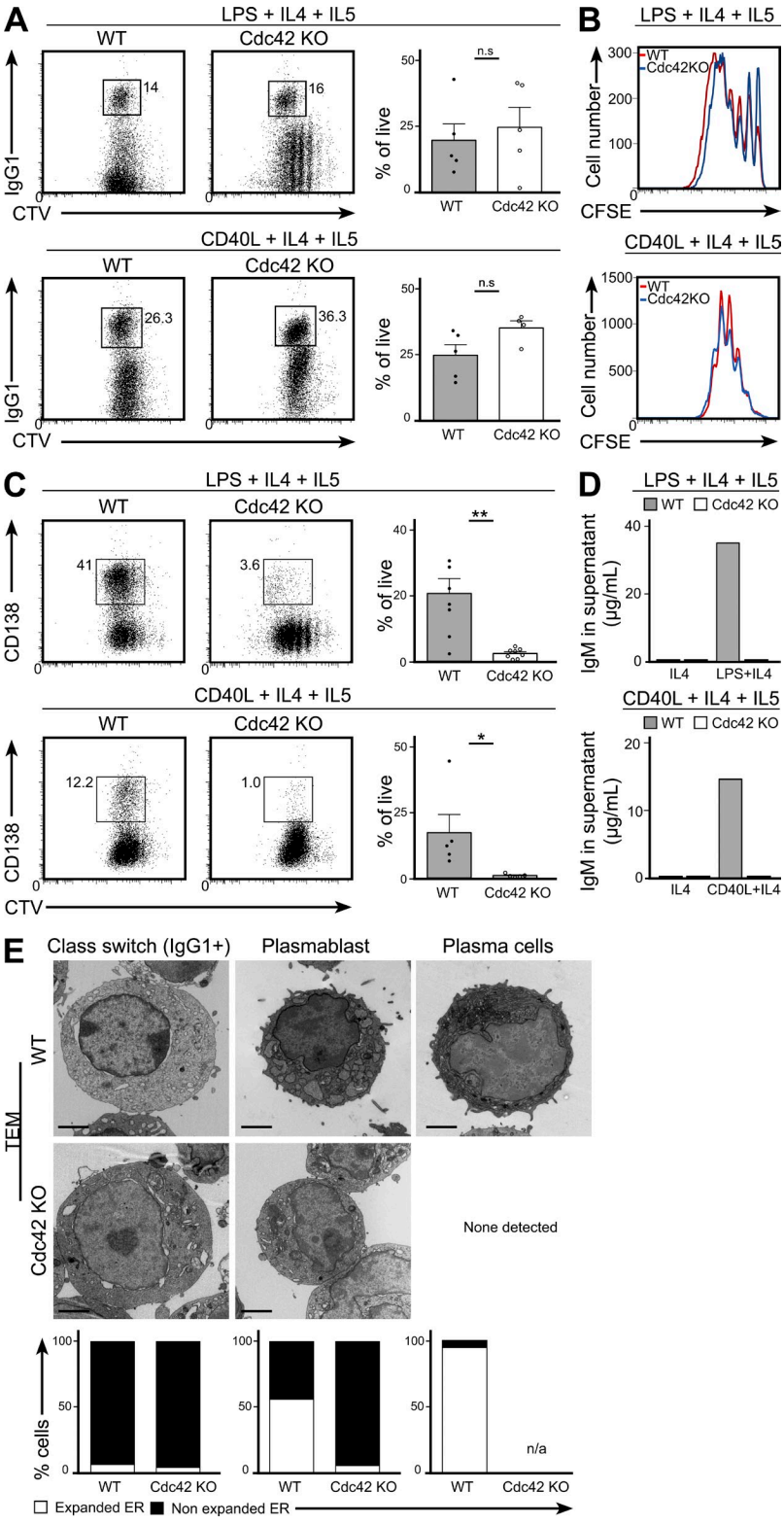

Figure 7. Plasma cell differentiation requires Cdc42. (A–E) CTV-labeled splenic WT and Cdc42 KO B cells were stimulated for 4 d with LPS or CD40L in the presence of IL-4 and IL-5. Flow cytometry was used to measure class switch recombination ($IgG1^+$ cells; A), proliferation (CTV dilution; B), and plasma cell differentiation ($CD138^{hi}$; C). Secreted IgM in culture supernatants was measured by sandwich ELISA (D). Cultured cells were sorted on the basis of IgG1 and CD138 expression as well as CTV dilution. Cells were then prepared for transmission electron microscopy (TEM). (E) Representative TEM images of $IgG1^+$ cells; plasmablasts ($IgG1^-CTV^{lo}CD138^{int}$), and plasma cells ($IgG1^-CTV^{lo}CD138^{hi}$) are shown. Quantitation of percentage of cells with expanded or nonexpanded ER is shown in graphs at the bottom. Data are representative at least 4 experiments with one mouse in each. Mean and SEM. Student's *t* test, *, $P < 0.05$; **, $P < 0.01$.

up-regulation of Blimp1 is a hallmark of plasma cell differentiation (Turner et al., 1994) and can be triggered by the transient expression of AP-1 transcription factors such as c-fos and c-jun after CD40L stimulation (Ohkubo et al., 2005). In line with this, we observed the transient expression of c-fos and c-jun in WT B cells, 30 to 60 min after stimulation with CD40L (Fig. 8 B). In contrast, the expression of the AP-1 transcription factors was dramatically impaired in Cdc42 KO B cells (Fig. 8 B), rendering them unable to initiate the up-regulation of Blimp1 required for plasma cell differentiation.

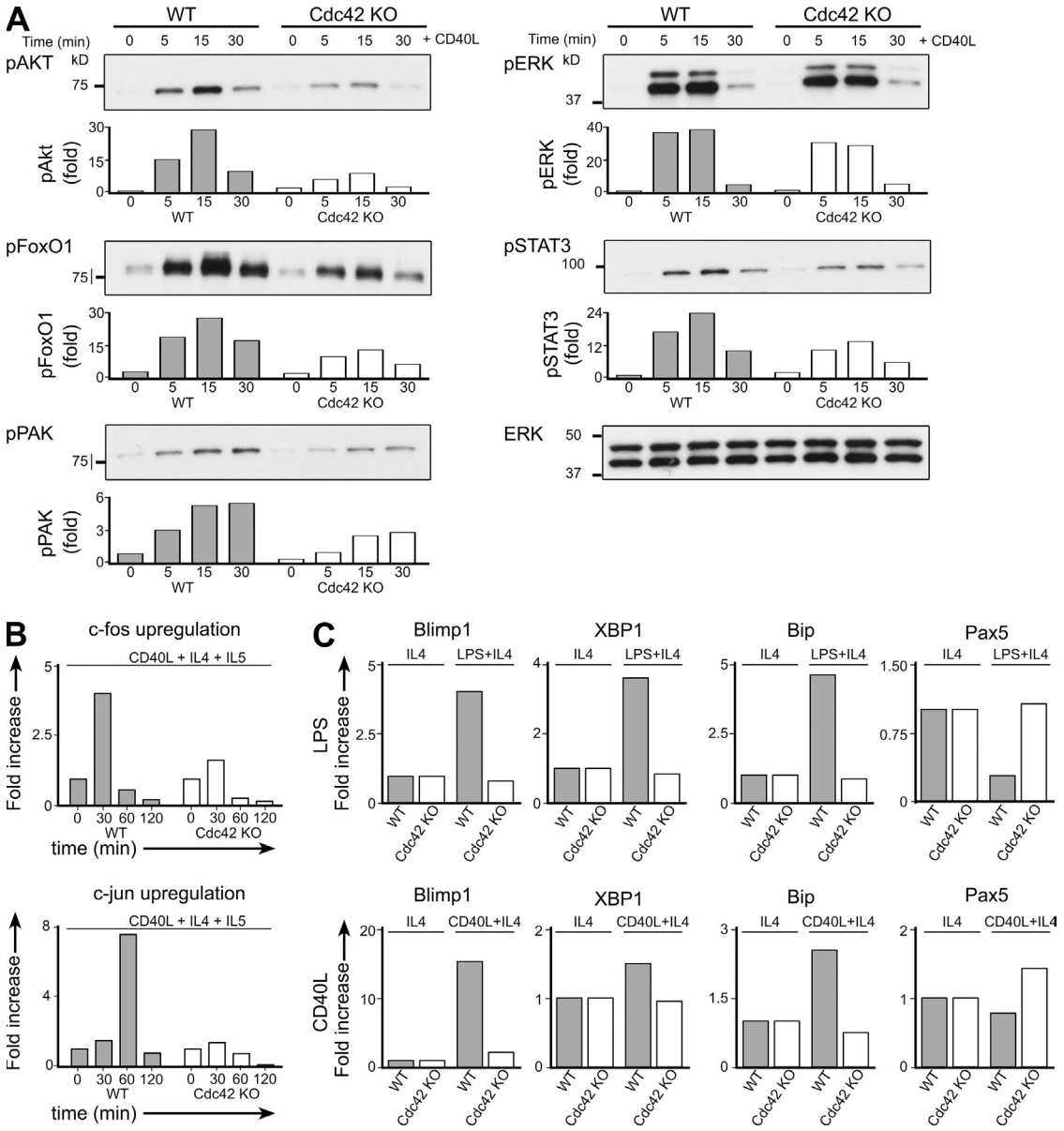

Figure 8. Cdc42 is required to initiate the plasma cell differentiation program. (A) Splenic WT and Cdc42 KO B cells were stimulated with CD40L for 30 min. Western blot analysis shows phosphorylation of Akt, FoxO1, Erk, STAT3, and PAK1. Quantifications shown in charts under blots indicate intensity of proteins relative to total Erk as determined by densitometry. (B and C) qRT-PCR for mRNA of indicated genes of WT or Cdc42 KO B cells stimulated for 0 –2 h (B) or for 4 d (C) with CD40L (B and C) or LPS (C) in the presence of IL-4 and IL-5. mRNA expression was normalized against the levels of carboxypeptidase H (CPH) and is presented as fold increase over the no stimulated condition (B) or cells treated with IL-4 and IL-5 only (C). Data are representative of 3 independent experiments.

To verify these findings, we also measured the expression levels of Blimp1 itself and its downstream targets XBP-1 and BiP using qRT-PCR. 4 d after stimulation with CD40L or LPS, WT B cells exhibit the up-regulation of Blimp1, XBP-1, and BiP that is characteristic of plasma cells (Fig. 8 C). However, Cdc42 KO B cells express significantly lower levels of each of these three markers while maintaining high expression levels of Pax5, a negative regulator of Blimp1 (Fig. 8 C). Collectively, these findings provide an underlying molecular explanation for the inability of Cdc42 KO B cells to initiate the plasma cell differentiation program.

Through our investigations, several different roles for the RhoGTPase Cdc42 in B cells have emerged, including participation in early BCR signaling, involvement in presentation of internalized antigen to T cells, and the formation of plasma cells. We anticipate that a combination of these various roles contributes to the inability of Cdc42 KO mice in mounting antibody responses after viral infection.

DISCUSSION

In this study, we have reevaluated the role of the small RhoGTPase Cdc42 in B cell physiology. We accomplished this through the generation of a new mouse model with a selective, early ablation of Cdc42 in the B cell compartment. This deletion of Cdc42 renders mice virtually unable to mount antibody responses after antigen immunization or viral infection. This immunodeficient phenotype appears to result from a combination of defects including: impaired signaling through the BCR, reduced antigen presentation to cognate T cells, and a severe block in plasma cell differentiation. Thus, and in contrast to previous studies, we have uncovered a fundamental role of Cdc42 in B cell development, activation and differentiation.

Our strategy for the B cell–specific deletion of Cdc42 involved crossing conditional targeted $Cdc42^{flox/flox}$ mice with mice expressing Cre-recombinase under the promoter of the *mb1* gene (Wu et al., 2006; Hobeika et al., 2006). This approach proved very effective with no apparent residual expression of Cdc42 in the mature B cell compartment as had previously been reported for CD19Cre (Rickert et al., 1997). Moreover, unlike previously reported mice that used the CD19 promoter for Cdc42 deletion (Guo et al., 2009), our mouse model allowed us to investigate the role of this RhoGTPase during very early events of B cell differentiation. Indeed, as Cdc42 KO bone marrow has fewer cells in Fraction C and a marked parenchymal retention of Fraction E cells compared with WT controls, it is clear that Cdc42 is involved in the early stages during B cell differentiation. The observed retention of maturing B cells in the parenchyma suggests an underlying defect in S1P-mediated egress into the sinusoids in the absence of Cdc42 (Pereira et al., 2010) and is in line with a reported role for Cdc42 in S1P signaling in Jurkat T cells (Kohno et al., 2003). Importantly, Cdc42 KO mice exhibit a dramatic diminution of recirculating mature B cells in the bone marrow, and a corresponding fourfold reduction in the numbers of mature B cells in the spleen and LNs. Furthermore, the deletion of Cdc42 also results in the complete absence of spleen marginal zone and peritoneum B cells (B1a, B1b, and B2). As such, our approach to selectively delete Cdc42 from B cells clearly demonstrates that Cdc42 participates at various stages during the development of B cells. However, it is worth noting that these roles for Cdc42 in B cell differentiation are distinct from those of other RhoGTPases and GEFs that are known to play a major role in B cell physiology. For instance, inactivation of the RhoGTPases Rac1 and Rac2 induces a block in B cell differentiation at the transitional stage (Walmsley et al., 2003), whereas deletion of the three Vav GEFs causes a blockage in the transition between the T1 and T2 stages, particularly in the follicular cell compartment (Doody et al., 2001; Fujikawa et al., 2003). Hence, our findings not only add to the increasing body of evidence highlighting the general importance of RhoGTPases during B cell development, but also establish an important and specific role for Cdc42 in this process.

In contrast to previous findings (Guo et al., 2009), we were somewhat surprised to observe that our *mb1*Cre Cdc42 KO mice exhibit almost undetectable levels of antibodies in the preimmune serum. Because we are working with different mice, we can only guess that this striking difference is the result of an incomplete deletion of Cdc42 by the CD19-cre used in their study. Our findings imply a fundamental role for Cdc42 in B cells in the antibody generation. In line with this, Cdc42 KO mice were unable to mount antibody responses against either antigen immunization or viral infections. We went on to dissect the molecular mechanisms that might underlie such a profoundly immunodeficient phenotype to better understand the roles that Cdc42 might play during B cell activation. Interestingly, we identified three distinct roles for Cdc42 in terms of BCR signaling, antigen presentation, and plasma cell differentiation. We assume that a combination of these three defects together may be sufficient to explain the dramatic phenotype observed on deletion of Cdc42 in the B cell compartment.

Antigen engagement of the BCR leads to activation of Src and Syk kinases (Kurosaki et al., 2010). Here, we found that Cdc42 is activated very rapidly after BCR engagement, suggesting that this RhoGTPase participates in the very early events after antigen recognition. Indeed, Cdc42 KO B cells exhibit lower levels of Src and Syk activation in response to BCR cross-linking compared with WT cells. In addition, the extent of the co-receptor CD19 phosphorylation and intracellular calcium signaling was lower in Cdc42 KO B cells. These observations are in line with reduced early signaling through the BCR (Takata et al., 1994). Similarly, as the phosphorylation of Erk and Akt was lower in Cdc42 KO B cells, we found that later BCR signaling through the MAPK and PI3K pathways, respectively, was also impaired in the absence of Cdc42. Thus, it appears that Cdc42 plays a significant role in mediating signaling after BCR engagement.

At this stage it remains unclear how Cdc42 itself becomes activated, though this is likely to occur through the activation of one or more GEFs. One likely candidate, GEFs, whose participation in signaling downstream of the BCR has been established is the Vav family of proteins (Zhang et al., 1995). This family of GEFs is activated by phosphorylation by Syk (Bustelo et al., 1992) and is thought to activate RacGTPases in response to BCR engagement. However, as B cells deficient in all three Vav family members are able to phosphorylate Erk to the same levels as WT B cells (Fujikawa et al., 2003), it seems that Cdc42 may be activated through a different pathway. Notably, we observed that BCR signaling in response to membrane-bound antigen was also impaired in the absence of Cdc42. As such, Cdc42 KO B cells were less able to spread on antigen-coated coverslips and antigen-loaded lipid bilayers. This is particularly interesting, given the well-established role of Cdc42 in regulating effectors associated with actin remodeling and the requirement for cytoskeleton reorganizations for this mode of antigen recognition. In view of this, although the precise sequence of events by which the BCR is activated remains a matter of debate (Pierce and Liu, 2010), it is tempting to speculate that the reduced capacity for early signal propagation might be a result of altered organization of

either IgM (Mattila et al., 2013; Kläsener et al., 2014) or of the cytoskeleton itself in B cells lacking Cdc42 (Treanor et al., 2010, 2011). In line with this suggestion, resting Cdc42 KO B cells exhibit significantly lower levels of F-actin compared with WT controls, though substantial future work will be required to formally establish our hypothesis.

One consequence of BCR signaling is the internalization of antigen into endosomal compartments for proteolytic cleavage, loading onto MHCII molecules, and subsequent presentation to cognate T cells (Amigorena et al., 1994; Lanzavecchia, 1985). In agreement with previous studies (Yuseff et al., 2011), we found that the process of BCR internalization was independent of Cdc42 in the case of soluble antigen with only a slight delay for particulate antigen. In contrast, the polarization of internalized antigen in endosomal compartments that has been reported (Siemasko et al., 1998) was remarkably impaired in the absence of Cdc42. As Cdc42 KO B cells are significantly less able to present internalized antigen on their surface, this suggests that Cdc42 plays a role in fusion and polarization of endosomes, and that this is important for efficient antigen presentation. Interestingly, the fusion of endosomal compartments has recently been linked both to the formation of the autophagosome (Chaturvedi et al., 2011) and asymmetric cell division (Thaunat et al., 2012). Furthermore, it has been suggested that the recruitment of lysosomes to the B cell synapse is necessary for extracellular degradation of antigen to facilitate extraction from the antigen-containing membrane (Yuseff et al., 2011). While the current study was performed using stimulation with soluble antigen, our findings support the notion that the polarization of antigen-containing endosomes occurs as a result of internal cues that are dependent on Cdc42. As such, these results not only corroborate Cdc42 as a master regulator of cell polarity but also reveal a potentially intriguing link between B cell polarity and antigen presentation.

Antigen in complex with MHCII on the B cell surface allows interaction with cognate $CD4^+$ T cells that provide the second signal required for B cell activation (Lanzavecchia, 1985). Here, we found that Cdc42 KO B cells are less able to present antigen to cognate T cells and as a result cannot proliferate to the same extent as WT B cells. Similarly, although Cdc42 KO B cells were able to mediate CCR7-dependent migration to the B/T cell border (Garside et al., 1998; Okada et al., 2005), and interact with T cells in vivo, the B–T cell conjugates formed were significantly shorter lived than those involving WT B cells. As sustained B–T cell conjugates are required for the formation of germinal centers and associated selection of B cells expressing high affinity BCR for antigen, this might provide a partial explanation for the immunodeficient phenotype observed in our Cdc42-deficient mice. However as Cdc42 KO B cells were able to form short-lived B–T cell conjugates, it seems likely that Cdc42 plays additional roles in mediating the production of antibodies in response to immunization with protein antigen or viral infection.

After activation, B cells proliferate and can undergo class switching and differentiation to form specialized plasma cells for the large-scale production of antibodies. We therefore investigated a possible role for Cdc42 in either class switching or plasma cell formation by using LPS or CD40L to override the BCR activation defects described above. Under these conditions, Cdc42 KO B cells were able to proliferate and class switch to the same extent as WT B cells. Nonetheless, we observed that in the absence of Cdc42 expression B cells were unable to differentiate to form plasma cells. One characteristic feature of plasma cells is the expression of Blimp-1 (Turner et al., 1994; Kallies et al., 2007), which induces the expression of genes including *XBP1* (Iwakoshi et al., 2003) and *HSPA5* (BiP; Shaffer et al., 2004) and the repression of several genes associated with B cell identity such as *PAX5* (Shaffer et al., 2002). Although the initiation of Blimp-1 expression is not fully understood, it has been suggested that members of the AP1 family of transcription factors, including c-fos and c-jun, can bind to the promoter and thereby regulate expression of the *prdm1* gene, which encodes Blimp-1 (Vasanwala et al., 2002; Ohkubo et al., 2005). In line with this suggestion, Cdc42 KO B cells were unable to initiate up-regulation of c-fos and c-jun to the levels seen in WT B cells in response to LPS or CD40L. This observation provides a possible molecular explanation as to why activated Cdc42-deficient B cells maintain expression of Pax5 and are unable to initiate the up-regulation of Blimp-1 required for plasma cell formation. However, in spite of the well-established role that players such as Blimp-1 have in the terminal differentiation of plasma cells, the signaling pathways by which their expression is regulated remains unclear. We observed that Cdc42 KO B cells exhibit lower levels of Akt and Foxo1 phosphorylation than WT cells after stimulation with CD40L. These findings are particularly interesting given the suggestion that the PI3K pathway participates in the regulation of both plasma cell differentiation and AID-dependent class switch recombination (Omori et al., 2006). Furthermore, we observed that in response to CD40L, Cdc42 KO B cells were less able to activate ERK and STAT3, two mediators that have been previously implicated in the differentiation of plasma cells (Yasuda et al., 2011). At this stage, although the precise regulatory signaling pathways remains elusive, it is clear that Cdc42 plays an important role in the formation of plasma cells after B cell activation.

Overall, by using an approach to delete Cdc42 in very early B cell progenitors, we have established a fundamental role for this RhoGTPase in several aspects of B cell biology, including B cell development, activation and plasma cell differentiation. We suggest that, combined, these Cdc42 functions culminate in the almost complete abrogation of antibody responses in our Cdc42 KO mouse model. This opens up new opportunities for the investigation and manipulation of antibody responses through this important GTPase.

MATERIALS AND METHODS

Animal breeding and generation. Mice with conditional deletion of Cdc42 in B cells were generated by backcrossing mice carrying a *Cdc42* allele floxed at exon 2 to mice expressing recombinase from the *mb1* promoter (coding for CD79a). Mice expressing the hen egg lysozyme–specific MD4 receptor were also crossed with Cdc42-floxed mice. OTII mice were used for purification of OVA-specific $CD4^+$ T cells. C57BL/6 mice were purchased

from The Jackson Laboratory. Mice were used between 8 and 10 wk of age. Cre^- littermates were used as WT controls.

Mice were bred and maintained at the animal facility of Cancer Research UK. All experiments were approved by the Animal Ethics Committee of Cancer Research UK and the UK Home Office.

Flow cytometry. Single-cell suspensions were prepared from spleen, LNs, bone marrow, or peritoneal lavage. After blocking Fc receptors using anti-CD16/32 antibodies, cells were stained with the appropriate combination of the following antibodies: B220 (RA3-6B2), TCRβ (H57-597), CD21 (7G6), CD4 (GK1.5), CD23 (B3B4), CD24 (M1/69), CD43 (S7), Ly-51 (6C3), B and T cell activation antigen (GL7), CD95 (Jo2), CD138 (281.2), IgG1 (A85.1), CD5 (53–7.3), CD11b (M1/70), CD19 (1D3), IgM (1B4B1 or II/41), and IgD (11–26).

For in vivo labeling, 1 µg phycoerythrin-labeled anti-CD45.2 was injected intravenously into recipients. After 2 min, animals were sacrificed.

For staining of intracellular signaling molecules, cells were fixed with 2% formaldehyde and permeabilized with ice-cold methanol for 30 min. Cells were then stained with primary antibodies against pSyk, pSrc, or pAkt, (all from Cell Signaling Technology), and then with secondary 555 anti–rabbit (Life Technologies) or, alternatively, with Alexa Fluor 647–labeled pErk (Phosflow; BD).

Data were acquired on LSR Fortessa (BD) and analyzed with FlowJo (Tree Star).

Beads preparation. 0.22-µm diam Alexa Fluor 647 streptavidin-coated beads (Bangs Laboratories) were incubated with a saturating amount of biotinylated anti-IgM (Southern Biotech) and OVA (EMD Millipore) or Eα peptide for 2 h at room temperature. Limiting stimulatory conditions were obtained by increasing the amounts of OVA or Eα peptide for coating, whereas IgM amounts were kept constant. Efficient titration of the IgM signal was measured by flow cytometry. Beads coated with anti-IgM alone were used for internalization assay.

Cell isolation, labeling and culture. Splenic naive B or CD4 T lymphocytes were purified using negative B cell or CD4 T cell isolation kits yielding enriched populations of ∼95–98% (B cells) and ∼80% (T cells), respectively (Miltenyi Biotec). Purified B or T cells were labeled in PBS with 2 µM CTV (Invitrogen), 2 µM SNARF1 (Invitrogen), or 1 µM CFSE (Invitrogen) for 10 min at 37°C. Cells were maintained in complete B cell medium (RPMI supplemented with 10% FCS, 25 mM Hepes, Glutamax, penicillin streptomycin [Invitrogen], and 1‰ β-mercaptoethanol [Sigma-Aldrich]).

Cdc42-GTP pull-down and immunoblotting. Purified B cells were left at 37°C for 10 min in chamber buffer (PBS, 0.5% FCS, 1 g/liter D-Glucose, 2 mM MgCl2, and 0.5 mM $CaCl_2$) to equilibrate before stimulation. They were then stimulated for various times with 10 µg/ml anti-IgM $F(ab')_2$ fragment (Jackson ImmunoResearch Laboratories), 10 µg/ml anti-κ (HB558; American Type Culture Collection), or 1 µg/ml CD40L (R&D Systems).

For Cdc42-GTP pull-down experiment, a commercial kit (Cytoskeleton Inc.) was used following the manufacturer's instructions, specifically using 10^7 B cells for 15 µg of beads. For immunoblotting, stimulated cells were then lysed in lysis buffer (20 mM Tris-HCL, pH 8.0,150 mM NaCl, 5 mM EDTA, Protease Inhibitor cocktail [Roche], 10 mM NaF, 1 mM Na_3VO_4, and 1% NP-40) for 15 min on ice, and samples were loaded into 4–20% (for Cdc42-GTP pull-down) or 12% (for all other applications) for electrophoresis. Proteins were detected with antibodies against pErk, pAkt (S473), pCD19, pSyk, pSrc, totalErk, pSTAT3 (Ser), and Cdc42 (all from Cell Signaling Technology) using the secondary HRP-conjugated anti–rabbit or anti–mouse antibodies (Jackson ImmunoResearch Laboratories).

Blot densitometry analysis was performed using the ImageJ (National Institutes of Health) software.

Proliferation analysis. CFSE- or CTV–labeled cells at a concentration of 10^6 cells per ml were stimulated in complete B cell medium supplemented with combinations of 10 µg LPS (Sigma-Aldrich) or 1 µg/ml CD40L (R&D Systems), 10 ng/ml of IL4 (R&D Systems), or 10 ng/ml of IL-5 (R&D Systems). CFSE or CTV dilution was measured after 4 d by flow cytometry.

For B-T cell co-culture, labeled B cells were loaded with fluorescent microspheres for 30 min at 37°C in complete medium, washed with complete medium to remove excess microspheres, and subsequently cultured with labeled OTII T cells in a 1:1 ratio.

Antigen internalization and presentation. For internalization assays, purified B cells were loaded with IgM coated beads or with soluble biotinylated anti-IgM (Southern Biotech) on ice for 30 min. Cells were then washed with PBS 2% FCS to remove excess antigen, and then incubated for 5–30 min at 37°C. After fixation with 2% paraformaldehyde, noninternalized beads were detected with Alexa Fluor 450 streptavidin (eBioscience).

To detect antigen presentation, B cells loaded with Ea peptide and IgM-coated beads were incubated between 3 and 5 h at 37°C, and then fixed in 2% formaldehyde. These cells were then stained with anti-MHCII/Ea antibody (eBioY-Ae; eBioscience), followed by anti–mouse IgG2b antibody staining (Life Technologies) for detection.

Optical microscopy. Planar lipid bilayers containing anti–mouse κ light chain (HB-58; American Type Culture Collection) were prepared in FCS2 chambers (Bioptechs Inc.) by liposome spreading as previously described (Carrasco et al., 2004). In brief, Alexa Fluor 633 streptavidin (Molecular Probes) was incorporated into lipid bilayers at density of 30 molecules/μm^2, to which monobiotinylated antigen was tethered. Assays were performed in chamber buffer at 37°C and imaged with TIRFM.

For spreading analysis, cells were settled on coverslips coated either with anti-κ chain antibody (HB-58; American Type Culture Collection), or anti-MHCII antibody (TIB120; American Type Culture Collection) at 37°C. After 10 min, cells were fixed with 2% paraformaldehyde, and then either prepared for scanning electron microscopy, or permeabilized with PBS 0.3% Triton and stained with Alexa Fluor 488 phalloidin (Molecular Probes).

TIRF images were acquired with an EMCCD camera (iXon3 897, Andor) coupled to a TIRF microscopy system (Cell R; Olympus) with 488-nm, 561-nm and 640-nm lasers (Olympus). Images were recorded with Cell R software (Olympus) and analyzed with ImageJ software (National Institutes of Health).

LNs and spleens were embedded in OCT and frozen in cold isopenthane and 10-µm-wide frozen sections were cut with a cryostat. Sections were fixed in 4% paraformaldehyde, blocked with PBS containing 1% BSA, and 10% goat serum (IF blocking buffer). Where stated, sections were also permeabilized with PBS 0.3% Triton for 3 min. Stainings were performed in IF blocking buffer with a combination of the following antibodies: Bcl6 PE, B220 PB (RA3-6B2), TCRβ FITC (H57-597), CD169 AF633 (Ser-4, ATCC), anti-κ PE (187.1), and F4/80 APC (BM8).

To examine polarization of antigen, purified B cells were incubated with Alexa Fluor 647 anti-IgM (Jackson ImmunoResearch Laboratories), and incubated for 30 min at 37°C. Cells were then settled on poly-L-lysine–coated 8-well glasses (C.A Hendley). After 10 min, cells were fixed with 2% 37°C warm PFA for 40 min, and then permeabilized with PBS 0.3% Triton, blocked for 1 h, and stained with Alexa Fluor 488 phalloidin and anti-tubulin antibody (Sigma-Aldrich), followed by Alexa Fluor 488 anti–mouse IgG1 (Life Technologies).

Confocal imaging was performed with a LSM 780 microscope (Carl Zeiss) with a plan apochromat 20×, NA 0.8 objective for tissue sections or a plan apochromat 63×, NA 1.40 objective for other applications. Images were analyzed with Imaris (Bitplane) and ImageJ softwares. For tissue sections, tiled images were acquired and assembled with the Zen software.

For multiphoton microscopy, explanted popliteal and inguinal LNs were prepared as previously described (Carrascoand Batista, 2007), and imaged with an upright multiphoton microscope (Olympus), a 25×, NA 1.05 water immersion objective, and a pulsed Ti:sapphire laser (Spectra Physics MaiTai HP DeepSee) tuned to 820 nm. Emission wavelengths were detected through band-pass filters of 420–500 nm (CTV), 515–560 nm (CFSE), and 590–650 nm

(SNARF-1). Multidimensional videos were analyzed with Imaris. Fluorescence bleed-through into the channel with longer wavelength was removed by subtracting the channel with shorter wavelength. Interaction times were measured using spot co-localization with a distance threshold of 10 µm. The arrest coefficient was calculated for each track as the percentage of the track length in which the cell moves less than 2 µm/min using Matlab (The MathWorks).

dSTORM super-resolution microscopy was performed as previously described (Mattila et al., 2013). In brief, cells were labeled with Cy5-conjugated Fab fragments (anti-IgM; Jackson ImmunoResearch Laboratories), and samples were fixed (4% paraformaldehyde, 0.2% glutaraldehyde in PBS) for 40 min and imaged in dSTORM switching buffer (PBS, pH 7.4; Sigma-Aldrich; 0.1 M β-mercaptoethylamine; Sigma-Aldrich) with colloidal gold particles (40 nm or 100 nm diameter; British Biocell) as fiducials. Imaging was performed on an Elyra PS1 microscope using TIRF with 640 and 405 nm excitation with a 100×, NA 1.46 α-plan apochromat. Localization tables were created using Zen software (Carl Zeiss) and used for image rendering and cluster analysis in Matlab. We defined a rectangular window of 3 µm side length around the center of the cells in which we used Ripley's K-derived H function (Kiskowski et al., 2009) as an established statistical tool (Zhang et al., 2006) to quantitatively analyze the clustering tendency, as previously described (Mattila et al., 2013).

Electron microscopy. For scanning electron microscopy, samples were initially fixed with double strength fixative, i.e., 8% (vol/vol) formaldehyde (TAAB Laboratories Equipment Ltd.) in 0.2 M phosphate buffer (PB), added directly to the cell culture medium (1:1) for 15 min. Samples were then fixed in 2.5% (vol/vol) glutaraldehyde (TAAB)/4% (vol/vol) formaldehyde in 0.1 M phosphate buffer (PB) for 30 min at room temperature, washed 3 × 5 min in PB, dehydrated stepwise through ethanol (2× 5 min 70, 90, and 100%), and critical point dried from liquid carbon dioxide using a Leica EM CPD300. Coverslips were then mounted on sticky carbon discs, sputter-coated with platinum, and viewed with at 5 kV and a working distance of ∼10 mm (Quanta FEG 250 Scanning Electron Microscope; FEI).

For transmission electron microscopy, cells were sorted into 4% paraformaldehyde (final concentration 2%) centrifuged gently (500 g) for 5 min and resuspended in 2.5% (vol/vol) glutaraldehyde/4% (vol/vol) formaldehyde in 0.1M phosphate buffer (PB) for 30 min. Cells were centrifuged again, post-fixed with 1% osmium tetroxide/1.5% potassium ferricyanide for 1 h at 4°C, stained with 1% tannic acid in 0.05 M PB for 45 min, followed by 1% sodium sulfate for 5 min. The pellets were dehydrated stepwise through ethanol (2× 10 min 70, 90, and 100%) and embedded in epon. Blocks were sectioned (UC6 ultramicrotome; Leica), picked up on Formvar-coated slot grids and post-stained with lead citrate. Sections were viewed using a transmission electron microscope (Tecnai G2 Spirit; FEI) and images were captured (Orius CCD; Gatan Inc).

Immunizations, infection, and ELISA. For immunization, mice were injected i.p. with 50 µg NP19-KLH (Biosearch Technology) in 4mg Alum (Thermo Fisher Scientific). Blood samples were taken from the lateral tail vein on day 0, 7, 14, 21, 28 after immunization.

For infection, mice were intranasally immunized with 200pfu of Influenza A virus (PR8 strain). Blood samples were taken from the lateral tail vein on day 0 and 9 after infection.

NP- or Influenza-specific antibody titers were detected by ELISA, using NP23-BSA, NP3-BSA, or live Influenza virus for capture, and biotinylated anti–mouse IgM (Southern Biotech), IgG (Southern Biotech), IgG2b (Southern Biotech), IgG2c (Southern Biotech), and IgG3 (BD). Titers were determined from the dilution curve in the linear range of absorbance.

Total antibody levels in serum before immunization were measured by sandwich ELISA. For capture, anti-IgM II/41 (BD), anti-IgG2b (BD), and anti-IgG2c (BD) were used. Purified IgM (BD), IgG2b (Southern Biotech), or IgG2c (Bethyl) were used as standards. Biotinylated antibodies were used for detection. For IgG1, a commercial kit was used (eBioscience).

All noncommercial ELISA plates were developed with alkaline-phosphatase streptavidin (Sigma-Aldrich) and phosphorylated nitrophenyl phosphate (Sigma-Aldrich). Absorbance at 405 nm was determined with a SPECTRAmax190 plate reader (Molecular Devices).

Quantitative RT-PCR. After stimulation with CD40L or LPS in the presence of IL4, 2×10^5 B cells were lysed and RNA was extracted using a RNA mini-kit following manufacturer's instruction, followed by reverse-transcription into cDNA with random hexamers from the SuperScript III First-Strand system (Invitrogen). Quantitative real-time PCR was performed using a ABI 7900T system and cDNA levels were detected using SybrGreen (Life Technologies). A list of the primers used can be found in Table S1.

Experimental data and statistical analysis. Sample sizes were chosen on the basis of published work in which similar phenotypical characterization and similar defects were reported. Cohort randomization or 'blinding' of investigators to sample identity was not done in this study. In some experiments, the data for each study group were compared with Student's *t* test and P-values were calculated. Normal distribution of samples was assumed on the basis of published studies with analyses similar to ours.

Online supplemental material. A list of primers used for qRT-PCR can be found in Table S1. Representative videos of spreading and contraction of WT or Cdc42 KO B cells on antigen-coated bilayers are presented in Videos 1 and 2, respectively. A representative video from homeostatic cell movement is presented in Video 3. A representative video showing interactions of WT and Cdc42 KO B cells with OTII T cells after immunization is presented in Video 4. Online supplemental material is available at http://www.jem.org/cgi/content/full/jem.20141143/DC1.

We thank the flow cytometry facility for cell sorting and the biological resource unit (Cancer Research UK). We thank Naomi E. Harwood (Cancer Research UK) for edition and critical reading of the manuscript. We thank David Mestre for help with preparing the figures. We thank all the members of the Lymphocyte Interaction Laboratory as well as Pieta K. Mattila (University of Turku) for critical reading of the manuscript. We thank Michael Reth for the *mb1*Cre strain.

This work was supported by Cancer Research UK, the German Research Foundation grant Ke1737/1-1 (S.J. Keppler), the Institute Pasteur-Fondazione Cenci Bolognetti (F. Gasparrini), a long-term fellowship from EMBO (N. Martínez-Martín), and a Royal Society Wolfson Research Merit Award (F.D. Batista).

The authors declare no competing financial interests.

Submitted: 17 June 2014
Accepted: 25 November 2014

REFERENCES

Amigorena, S., J.R. Drake, P. Webster, and I. Mellman. 1994. Transient accumulation of new class II MHC molecules in a novel endocytic compartment in B lymphocytes. *Nature*. 369:113–120. http://dx.doi.org/10.1038/369113a0

Arana, E., A. Vehlow, N.E. Harwood, E. Vigorito, R. Henderson, M. Turner, V.L.J. Tybulewicz, and F.D. Batista. 2008. Activation of the small GTPase Rac2 via the B cell receptor regulates B cell adhesion and immunological-synapse formation. *Immunity*. 28:88–99. http://dx.doi.org/10.1016/j.immuni.2007.12.003

Aspenström, P., U. Lindberg, and A. Hall. 1996. Two GTPases, Cdc42 and Rac, bind directly to a protein implicated in the immunodeficiency disorder Wiskott-Aldrich syndrome. *Curr. Biol.* 6:70–75. http://dx.doi.org/10.1016/S0960-9822(02)00423-2

Batista, F.D., and N.E. Harwood. 2009. The who, how and where of antigen presentation to B cells. *Nat. Rev. Immunol.* 9:15–27. http://dx.doi.org/10.1038/nri2454

Becker-Herman, S., A. Meyer-Bahlburg, M.A. Schwartz, S.W. Jackson, K.L. Hudkins, C. Liu, B.D. Sather, S. Khim, D. Liggitt, W. Song, et al. 2011.

WASp-deficient B cells play a critical, cell-intrinsic role in triggering autoimmunity. *J. Exp. Med.* 208:2033–2042. http://dx.doi.org/10.1084/jem.20110200

Brezski, R.J., and J.G. Monroe. 2007. B cell antigen receptor-induced Rac1 activation and Rac1-dependent spreading are impaired in transitional immature B cells due to levels of membrane cholesterol. *J. Immunol.* 179:4464–4472. http://dx.doi.org/10.4049/jimmunol.179.7.4464

Bustelo, X.R., J.A. Ledbetter, and M. Barbacid. 1992. Product of vav proto-oncogene defines a new class of tyrosine protein kinase substrates. *Nature.* 356:68–71. http://dx.doi.org/10.1038/356068a0

Carrasco, Y.R., and F.D. Batista. 2007. B cells acquire particulate antigen in a macrophage-rich area at the boundary between the follicle and the subcapsular sinus of the lymph node. *Immunity.* 27:160–171. doi:10.1016/j.immuni.2007.06.007

Carrasco, Y.R., S.J. Fleire, T. Cameron, M.L. Dustin, and F.D. Batista. 2004. LFA-1/ICAM-1 interaction lowers the threshold of B cell activation by facilitating B cell adhesion and synapse formation. *Immunity.* 20:589–599.

Chaturvedi, A., R. Martz, D. Dorward, M. Waisberg, and S.K. Pierce. 2011. Endocytosed BCRs sequentially regulate MAPK and Akt signaling pathways from intracellular compartments. *Nat. Immunol.* 12:1119–1126. http://dx.doi.org/10.1038/ni.2116

Depoil, D., S. Fleire, B.L. Treanor, M. Weber, N.E. Harwood, K.L. Marchbank, V.L.J. Tybulewicz, and F.D. Batista. 2008. CD19 is essential for B cell activation by promoting B cell receptor-antigen microcluster formation in response to membrane-bound ligand. *Nat. Immunol.* 9:63–72. http://dx.doi.org/10.1038/ni1547

Derry, J.M., H.D. Ochs, and U. Francke. 1994. Isolation of a novel gene mutated in Wiskott-Aldrich syndrome. *Cell.* 79:922.

Doody, G.M., S.E. Bell, E. Vigorito, E. Clayton, S. McAdam, R. Tooze, C. Fernandez, I.J. Lee, and M. Turner. 2001. Signal transduction through Vav-2 participates in humoral immune responses and B cell maturation. *Nat. Immunol.* 2:542–547. http://dx.doi.org/10.1038/88748

Etienne-Manneville, S. 2004. Cdc42 - the centre of polarity. *J. Cell Sci.* 117: 1291–1300.

Fleire, S.J., J.P. Goldman, Y.R. Carrasco, M. Weber, D. Bray, and F.D. Batista. 2006. B cell ligand discrimination through a spreading and contraction response. *Science.* 312:738–741. http://dx.doi.org/10.1126/science.1123940

Fujikawa, K., A.V. Miletic, F.W. Alt, R. Faccio, T. Brown, J. Hoog, J. Fredericks, S. Nishi, S. Mildiner, S.L. Moores, et al. 2003. Vav1/2/3-null mice define an essential role for Vav family proteins in lymphocyte development and activation but a differential requirement in MAPK signaling in T and B cells. *J. Exp. Med.* 198:1595–1608. http://dx.doi.org/10.1084/jem.20030874

Garside, P., E. Ingulli, R.R. Merica, J.G. Johnson, R.J. Noelle, and M.K. Jenkins. 1998. Visualization of specific B and T lymphocyte interactions in the lymph node. *Science.* 281:96–99. http://dx.doi.org/10.1126/science.281.5373.96

Goodnow, C.C., J. Crosbie, S. Adelstein, T.B. Lavoie, S.J. Smith-Gill, R.A. Brink, H. Pritchard-Briscoe, J.S. Wotherspoon, R.H. Loblay, K. Raphael, et al. 1988. Altered immunoglobulin expression and functional silencing of self-reactive B lymphocytes in transgenic mice. *Nature.* 334:676–682. http://dx.doi.org/10.1038/334676a0

Guo, F., C.S. Velu, H.L. Grimes, and Y. Zheng. 2009. Rho GTPase Cdc42 is essential for B-lymphocyte development and activation. *Blood.* 114:2909–2916. http://dx.doi.org/10.1182/blood-2009-04-214676

Hao, S., and A. August. 2005. Actin depolymerization transduces the strength of B-cell receptor stimulation. *Mol. Biol. Cell.* 16:2275–2284. http://dx.doi.org/10.1091/mbc.E04-10-0881

Hardy, R.R., C.E. Carmack, S.A. Shinton, J.D. Kemp, and K. Hayakawa. 1991. Resolution and characterization of pro-B and pre-pro-B cell stages in normal mouse bone marrow. *J. Exp. Med.* 173:1213–1225. http://dx.doi.org/10.1084/jem.173.5.1213

Hobeika, E., S. Thiemann, B. Storch, H. Jumaa, P.J. Nielsen, R. Pelanda, and M. Reth. 2006. Testing gene function early in the B cell lineage in mb1-cre mice. *Proc. Natl. Acad. Sci. USA.* 103:13789–13794. http://dx.doi.org/10.1073/pnas.0605944103

Iwakoshi, N.N., A.-H. Lee, P. Vallabhajosyula, K.L. Otipoby, K. Rajewsky, and L.H. Glimcher. 2003. Plasma cell differentiation and the unfolded protein response intersect at the transcription factor XBP-1. *Nat. Immunol.* 4:321–329. http://dx.doi.org/10.1038/ni907

Johnson, D.I., and J.R. Pringle. 1990. Molecular characterization of CDC42, a *Saccharomyces cerevisiae* gene involved in the development of cell polarity. *J. Cell Biol.* 111:143–152. http://dx.doi.org/10.1083/jcb.111.1.143

Kallies, A., J. Hasbold, K. Fairfax, C. Pridans, D. Emslie, B.S. McKenzie, A.M. Lew, L.M. Corcoran, P.D. Hodgkin, D.M. Tarlinton, and S.L. Nutt. 2007. Initiation of plasma-cell differentiation is independent of the transcription factor Blimp-1. *Immunity.* 26:555–566. http://dx.doi.org/10.1016/j.immuni.2007.04.007

Kiskowski, M.A., J.F. Hancock, and A.K. Kenworthy. 2009. On the use of Ripley's K-function and its derivatives to analyze domain size. *Biophys. J.* 97:1095–1103. http://dx.doi.org/10.1016/j.bpj.2009.05.039

Kläsener, K., P.C. Maity, E. Hobeika, J. Yang, and M. Reth. 2014. B cell activation involves nanoscale receptor reorganizations and inside-out signaling by Syk. *eLife.* 3:e02069. http://dx.doi.org/10.7554/eLife.02069

Kohno, T., H. Matsuyuki, Y. Inagaki, and Y. Igarashi. 2003. Sphingosine 1-phosphate promotes cell migration through the activation of Cdc42 in Edg-6/S1P4-expressing cells. *Genes Cells.* 8:685–697. http://dx.doi.org/10.1046/j.1365-2443.2003.00667.x

Kolluri, R., K.F. Tolias, C.L. Carpenter, F.S. Rosen, and T. Kirchhausen. 1996. Direct interaction of the Wiskott-Aldrich syndrome protein with the GTPase Cdc42. *Proc. Natl. Acad. Sci. USA.* 93:5615–5618. http://dx.doi.org/10.1073/pnas.93.11.5615

Kurosaki, T., H. Shinohara, and Y. Baba. 2010. B cell signaling and fate decision. *Annu. Rev. Immunol.* 28:21–55. http://dx.doi.org/10.1146/annurev.immunol.021908.132541

Lanzavecchia, A. 1985. Antigen-specific interaction between T and B cells. *Nature.* 314:537–539. http://dx.doi.org/10.1038/314537a0

Liu, C., X. Bai, J. Wu, S. Sharma, A. Upadhyaya, C.I.M. Dahlberg, L.S. Westerberg, S.B. Snapper, X. Zhao, and W. Song. 2013. N-wasp is essential for the negative regulation of B cell receptor signaling. *PLoS Biol.* 11:e1001704. http://dx.doi.org/10.1371/journal.pbio.1001704

Mattila, P.K., C. Feest, D. Depoil, B. Treanor, B. Montaner, K.L. Otipoby, R. Carter, L.B. Justement, A. Bruckbauer, and F.D. Batista. 2013. The actin and tetraspanin networks organize receptor nanoclusters to regulate B cell receptor-mediated signaling. *Immunity.* 38:461–474. http://dx.doi.org/10.1016/j.immuni.2012.11.019

Miller, M.J., S.H. Wei, I. Parker, and M.D. Cahalan. 2002. Two-photon imaging of lymphocyte motility and antigen response in intact lymph node. *Science.* 296:1869–1873. http://dx.doi.org/10.1126/science.1070051

Ohkubo, Y., M. Arima, E. Arguni, S. Okada, K. Yamashita, S. Asari, S. Obata, A. Sakamoto, M. Hatano, J. O-Wang, et al. 2005. A role for c-fos/activator protein 1 in B lymphocyte terminal differentiation. *J. Immunol.* 174:7703–7710. http://dx.doi.org/10.4049/jimmunol.174.12.7703

Okada, T., M.J. Miller, I. Parker, M.F. Krummel, M. Neighbors, S.B. Hartley, A. O'Garra, M.D. Cahalan, and J.G. Cyster. 2005. Antigen-engaged B cells undergo chemotaxis toward the T zone and form motile conjugates with helper T cells. *PLoS Biol.* 3:e150. http://dx.doi.org/10.1371/journal.pbio.0030150

Omori, S.A., M.H. Cato, A. Anzelon-Mills, K.D. Puri, M. Shapiro-Shelef, K. Calame, and R.C. Rickert. 2006. Regulation of class-switch recombination and plasma cell differentiation by phosphatidylinositol 3-kinase signaling. *Immunity.* 25:545–557. http://dx.doi.org/10.1016/j.immuni.2006.08.015

Pereira, J.P., J. An, Y. Xu, Y. Huang, and J.G. Cyster. 2009. Cannabinoid receptor 2 mediates the retention of immature B cells in bone marrow sinusoids. *Nat. Immunol.* 10:403–411. http://dx.doi.org/10.1038/ni.1710

Pereira, J.P., Y. Xu, and J.G. Cyster. 2010. A role for S1P and S1P1 in immature-B cell egress from mouse bone marrow. *PLoS ONE.* 5:e9277. http://dx.doi.org/10.1371/journal.pone.0009277

Pierce, S.K., and W. Liu. 2010. The tipping points in the initiation of B cell signalling: how small changes make big differences. *Nat. Rev. Immunol.* 10:767–777. http://dx.doi.org/10.1038/nri2853

Rajewsky, K. 1996. Clonal selection and learning in the antibody system. *Nature.* 381:751–758. http://dx.doi.org/10.1038/381751a0

Randall, K.L., T. Lambe, A.L. Johnson, B. Treanor, E. Kucharska, H. Domaschenz, B. Whittle, L.E. Tze, A. Enders, T.L. Crockford, et al. 2009. Dock8 mutations cripple B cell immunological synapses, germinal centers and long-lived antibody production. *Nat. Immunol.* 10:1283–1291. http://dx.doi.org/10.1038/ni.1820

Rickert, R.C., J. Roes, and K. Rajewsky. 1997. B lymphocyte-specific, Cre-mediated mutagenesis in mice. *Nucleic Acids Res.* 25:1317–1318. http://dx.doi.org/10.1093/nar/25.6.1317

Rudensky AYu, S., P. Rath, D.B. Preston-Hurlburt, Murphy, and C.A. Janeway Jr. 1991. On the complexity of self. *Nature*. 353:660–662. http://dx.doi.org/10.1038/353660a0

Saci, A., and C.L. Carpenter. 2005. RhoA GTPase regulates B cell receptor signaling. *Mol. Cell*. 17:205–214. http://dx.doi.org/10.1016/j.molcel.2004.12.012

Shaffer, A.L., K.-I. Lin, T.C. Kuo, X. Yu, E.M. Hurt, A. Rosenwald, J.M. Giltnane, L. Yang, H. Zhao, K. Calame, and L.M. Staudt. 2002. Blimp-1 orchestrates plasma cell differentiation by extinguishing the mature B cell gene expression program. *Immunity*. 17:51–62. http://dx.doi.org/10.1016/S1074-7613(02)00335-7

Shaffer, A.L., M. Shapiro-Shelef, N.N. Iwakoshi, A.-H. Lee, S.-B. Qian, H. Zhao, X. Yu, L. Yang, B.K. Tan, A. Rosenwald, et al. 2004. XBP1, downstream of Blimp-1, expands the secretory apparatus and other organelles, and increases protein synthesis in plasma cell differentiation. *Immunity*. 21:81–93. http://dx.doi.org/10.1016/j.immuni.2004.06.010

Siemasko, K., B.J. Eisfelder, E. Williamson, S. Kabak, and M.R. Clark. 1998. Cutting edge: signals from the B lymphocyte antigen receptor regulate MHC class II containing late endosomes. *J. Immunol*. 160:5203–5208.

Sohn, H.W., P. Tolar, and S.K. Pierce. 2008. Membrane heterogeneities in the formation of B cell receptor-Lyn kinase microclusters and the immune synapse. *J. Cell Biol.* 182:367–379. http://dx.doi.org/10.1083/jcb.200802007

Sullivan, K.E., C.A. Mullen, R.M. Blaese, and J.A. Winkelstein. 1994. A multiinstitutional survey of the Wiskott-Aldrich syndrome. *J. Pediatr.* 125:876–885. http://dx.doi.org/10.1016/S0022-3476(05)82002-5

Symons, M., J.M. Derry, B. Karlak, S. Jiang, V. Lemahieu, F. Mccormick, U. Francke, and A. Abo. 1996. Wiskott-Aldrich syndrome protein, a novel effector for the GTPase CDC42Hs, is implicated in actin polymerization. *Cell*. 84:723–734. http://dx.doi.org/10.1016/S0092-8674(00)81050-8

Takata, M., H. Sabe, A. Hata, T. Inazu, Y. Homma, T. Nukada, H. Yamamura, and T. Kurosaki. 1994. Tyrosine kinases Lyn and Syk regulate B cell receptor-coupled Ca2+ mobilization through distinct pathways. *EMBO J.* 13:1341–1349.

Thaunat, O., A.G. Granja, P. Barral, A. Filby, B. Montaner, L. Collinson, N. Martínez-Martin, N.E. Harwood, A. Bruckbauer, and F.D. Batista. 2012. Asymmetric segregation of polarized antigen on B cell division shapes presentation capacity. *Science*. 335:475–479. http://dx.doi.org/10.1126/science.1214100

Treanor, B., D. Depoil, A. Gonzalez-Granja, P. Barral, M. Weber, O. Dushek, A. Bruckbauer, and F.D. Batista. 2010. The membrane skeleton controls diffusion dynamics and signaling through the B cell receptor. *Immunity*. 32:187–199. http://dx.doi.org/10.1016/j.immuni.2009.12.005

Treanor, B., D. Depoil, A. Bruckbauer, and F.D. Batista. 2011. Dynamic cortical actin remodeling by ERM proteins controls BCR microcluster organization and integrity. *J. Exp. Med.* 208:1055–1068. http://dx.doi.org/10.1084/jem.20101125

Turner, C.A. Jr., D.H. Mack, and M.M. Davis. 1994. Blimp-1, a novel zinc finger-containing protein that can drive the maturation of B lymphocytes into immunoglobulin-secreting cells. *Cell*. 77:297–306. http://dx.doi.org/10.1016/0092-8674(94)90321-2

Tybulewicz, V.L.J., and R.B. Henderson. 2009. Rho family GTPases and their regulators in lymphocytes. *Nat. Rev. Immunol.* 9:630–644. http://dx.doi.org/10.1038/nri2606

Vasanwala, F.H., S. Kusam, L.M. Toney, and A.L. Dent. 2002. Repression of AP-1 function: a mechanism for the regulation of Blimp-1 expression and B lymphocyte differentiation by the B cell lymphoma-6 protooncogene. *J. Immunol.* 169:1922–1929. http://dx.doi.org/10.4049/jimmunol.169.4.1922

Vinuesa, C.G., and J.G. Cyster. 2011. How T cells earn the follicular rite of passage. *Immunity*. 35:671–680. http://dx.doi.org/10.1016/j.immuni.2011.11.001

Walmsley, M.J., S.K.T. Ooi, L.F. Reynolds, S.H. Smith, S. Ruf, A. Mathiot, L. Vanes, D.A. Williams, M.P. Cancro, and V.L.J. Tybulewicz. 2003. Critical roles for Rac1 and Rac2 GTPases in B cell development and signaling. *Science*. 302:459–462. http://dx.doi.org/10.1126/science.1089709

Weber, M., B. Treanor, D. Depoil, H. Shinohara, N.E. Harwood, M. Hikida, T. Kurosaki, and F.D. Batista. 2008. Phospholipase C-γ2 and Vav cooperate within signaling microclusters to propagate B cell spreading in response to membrane-bound antigen. *J. Exp. Med.* 205:853–868. http://dx.doi.org/10.1084/jem.20072619

Westerberg, L., G. Greicius, S.B. Snapper, P. Aspenström, and E. Severinson. 2001. Cdc42, Rac1, and the Wiskott-Aldrich syndrome protein are involved in the cytoskeletal regulation of B lymphocytes. *Blood*. 98:1086–1094. http://dx.doi.org/10.1182/blood.V98.4.1086

Westerberg, L.S., C. Dahlberg, M. Baptista, C.J. Moran, C. Detre, M. Keszei, M.A. Eston, F.W. Alt, C. Terhorst, L.D. Notarangelo, and S.B. Snapper. 2012. Wiskott-Aldrich syndrome protein (WASP) and N-WASP are critical for peripheral B-cell development and function. *Blood*. 119:3966–3974. http://dx.doi.org/10.1182/blood-2010-09-308197

Wu, X., F. Quondamatteo, T. Lefever, A. Czuchra, H. Meyer, A. Chrostek, R. Paus, L. Langbein, and C. Brakebusch. 2006. Cdc42 controls progenitor cell differentiation and beta-catenin turnover in skin. *Genes Dev.* 20:571–585. http://dx.doi.org/10.1101/gad.361406

Yasuda, T., K. Kometani, N. Takahashi, Y. Imai, Y. Aiba, and T. Kurosaki. 2011. ERKs induce expression of the transcriptional repressor Blimp-1 and subsequent plasma cell differentiation. *Sci. Signal.* 4:ra25. http://dx.doi.org/10.1126/scisignal.2001592

Yuseff, M.-I., A. Reversat, D. Lankar, J. Diaz, I. Fanget, P. Pierobon, V. Randrian, N. Larochette, F. Vascotto, C. Desdouets, et al. 2011. Polarized secretion of lysosomes at the B cell synapse couples antigen extraction to processing and presentation. *Immunity*. 35:361–374. http://dx.doi.org/10.1016/j.immuni.2011.07.008

Zhang, R., F.W. Alt, L. Davidson, S.H. Orkin, and W. Swat. 1995. Defective signalling through the T- and B-cell antigen receptors in lymphoid cells lacking the vav proto-oncogene. *Nature*. 374:470–473. http://dx.doi.org/10.1038/374470a0

Zhang, J., K. Leiderman, J.R. Pfeiffer, B.S. Wilson, J.M. Oliver, and S.L. Steinberg. 2006. Characterizing the topography of membrane receptors and signaling molecules from spatial patterns obtained using nanometer-scale electron-dense probes and electron microscopy. *Micron*. 37:14–34. http://dx.doi.org/10.1016/j.micron.2005.03.014

Zhang, Q., J.C. Davis, I.T. Lamborn, A.F. Freeman, H. Jing, A.J. Favreau, H.F. Matthews, J. Davis, M.L. Turner, G. Uzel, et al. 2009. Combined immunodeficiency associated with DOCK8 mutations. *N. Engl. J. Med.* 361:2046–2055. http://dx.doi.org/10.1056/NEJMoa0905506